DNA damage-induced nuclear import of HSP90α is promoted by Aha1

Nupur Fangaria[a], Khushboo Rani[a], Priyanka Singh[a], Sandeep Dey[b], Kota Arun Kumar[b], and Sunanda Bhattacharyya[a,*]

[a]Department of Biotechnology and Bioinformatics, School of Life Sciences, University of Hyderabad, Hyderabad 500046, Telangana, India; [b]Department of Animal Biology, School of Life Sciences, University of Hyderabad, Hyderabad 500046, Telangana, India

ABSTRACT **The interplay between yHSP90α (Hsp82) and Rad51 has been implicated in the DNA double-strand break repair (DSB) pathway in yeast. Here we report that nuclear translocation of yHSP90α and its recruitment to the DSB end are essential for homologous recombination (HR)-mediated DNA repair in yeast. The HsHSP90α possesses an amino-terminal extension which is phosphorylated upon DNA damage. We find that the absence of the amino-terminal extension in yHSP90α does not compromise its nuclear import, and the non-phosphorylatable-mutant HsHSP90α^{T7A} could be imported to the yeast nucleus upon DNA damage. Interestingly, the flexible charged-linker (CL) domains of both yHSP90α and HsHSP90α play a critical role during their nuclear translocation. The conformational restricted CL mutant yHSP90α$^{\Delta(211\text{-}259)}$, but not a shorter deletion version yHSP90α$^{\Delta(211\text{-}242)}$, fails to reach the nucleus. As the CL domain of yHSP90α is critical for its interaction with Aha1, we investigated whether Aha1 promotes the nuclear import of yHSP90α. We found that the nuclear import of yHSP90α is severely affected in Δ*aha1* strain. Moreover, Aha1 is accumulated in the nucleus during DNA damage. Hence Aha1 may serve as a potential target for inhibiting nuclear function of yHSP90α. The increased sensitivity of Δ*aha1* strain to genotoxic agents strengthens this notion.**

Monitoring Editor
Karsten Weis
ETH Zurich

Received: Nov 5, 2021
Revised: Sep 29, 2022
Accepted: Oct 11, 2022

INTRODUCTION

Eukaryotic cells are susceptible to a wide variety of genotoxic stresses which cause several types of DNA lesions including DNA double-strand breaks (DSBs). If DSBs remain unrepaired in the cell, they can cause genomic instability (Aylon and Kupiec, 2004). One of the commonly employed mechanisms to repair DSB is by homologous recombination (HR). Unlike the mammalian system, this mode of DNA repair is preferred in budding yeast over the error-prone nonhomologous end joining pathway. In HR-mediated DNA repair, Rad52 and Rad51 are assembled at the 3′ ssDNA tail in an organized manner (Li and Heyer, 2008). These proteins are recruited during the end resection of DNA DSB and catalyze the formation of DNA (Andriuskevicius *et al.*, 2018). Studies in the model eukaryote, *Saccharomyces cerevisiae*, have shown that yHSP90α, the budding yeast ortholog of human HSP90α (HsHSP90α), provides stability to Rad51 protein and plays a regulatory role in the effective recruitment of Rad51 to the broken DNA (Suhane *et al.*, 2014, 2019).

HSP90α is associated with a wide variety of cochaperones that are essential for its reaction cycle. Sba1 binds to HSP90α in the presence of ATP and stabilizes the ATP bound conformation which is required for the client protein activation (Ali *et al.*, 2006). Cdc37 aids in folding and activation of specific client protein kinases. It suppresses the ATP turnover by HSP90α and thereby helps in client protein loading (Kimura *et al.*, 1997; Siligardi *et al.*, 2002). Aha1

This article was published online ahead of print in MBoC in Press (http://www.molbiolcell.org/cgi/doi/10.1091/mbc.E21-11-0554) on October 19, 2022.

Conflict of interest: The authors declare no conflicts of interest.

Author contributions: S.B. conceived the idea, designed the experiments, guided, and wrote the paper; N.F. conducted experiments and wrote the paper; K.R. and P.S. conducted experiments; N.F., S.D., and K.A.K. conducted the fluorescence microscopic studies.

Funding: The work was supported by the Department of Science and Engineering Research Board (DST-SERB), India [EMR/2017/001173] to S.B.

All supporting data in relation to the studies reported here are provided in this manuscript.

*Address correspondence to: Sunanda Bhattacharyya (sdeb70@gmail.com; sbtsl@uohyd.ac.in).

Abbreviations used: Aha1, activator of hsp90 ATPase; Cdc37, cell division cycle 37; HOcs, homothallic endonuclease cut site; Hsp90, heat shock protein 90; Sba1, sensitivity to benzoquinone ansamycins.

accelerates the ATPase activity of HSP90α and plays an important role in regulating the timing of HSP90α chaperone cycle (Kimura *et al.*, 1997). Upon binding to the middle domain (MD) of HSP90α, Aha1 causes a large conformational change to the amino terminal domain (NTD) of HSP90α and acts as an allosteric activator of HSP90α ATPase. Subsequently, monomeric Aha1 binds asymmetrically to the NTD of one of the protomers of HSP90α and accelerates the dimerization of HSP90α by forming a bridge between the two protomers (Li *et al.*, 2012). Although the contribution of cochaperones toward the conformational cycle of HSP90α is well understood, their physiological significance remains obscure. Previous studies have indicated the involvement of the above-mentioned cochaperones in the DNA repair pathways in general (Caplan *et al.,* 2007; Echtenkamp *et al.,* 2011; Sun *et al.,* 2012). In HeLa cell extracts, Aha1 was found to interact with the proteins Ku70 and Ku80 and DNA-dependent protein kinase (DNA-PK)cs which are involved in DNA repair (Sun *et al.,* 2012). The Sba1 network was found to have a significant nuclear component that includes DNA repair activities (Echtenkamp *et al.,* 2011). A previous study showed that Δ*sba1* strain shows susceptibility toward various DNA-damaging agents like MMS, bleomycin, and ultraviolet light, which could be reversed by the complementation of Sba1 in the null Δ*sba1* cell. Loss of function of Cdc37 causes synthetic growth defect with several genes involved in genome integrity (Caplan *et al.,* 2007). Although previous studies indicate that these cochaperones may play a role in DNA repair, their exact function during the HR pathway has never been addressed.

During its chaperone cycle, HSP90α undergoes large-scale conformational rearrangements from an open inactive state to a closed active state (Mader *et al.*, 2020) which in turn modulates its catalytic activity. The NTD and the MD are separated by a disordered region termed the charged linker (CL), which provides flexibility for the domain rearrangement during the HSP90α chaperone cycle (Tsutsumi *et al.,* 2012). This linker region is evolutionarily conserved among all eukaryotic orthologs of HSP90α studied to date, although its physiological significance is poorly understood. To address the importance of CL domain in the mechanism of the in vitro function of HSP90α, a series of successively shortened CL mutants of yHSP90α were generated (Hainzl *et al.*, 2009). It was observed that successive deletion of CL gradually reduces the ability of Aha1 to stimulate the ATP turnover in the mutants without altering its binding affinity to those mutants (Hainzl *et al.*, 2009). It was reported that Aha1-mediated ATPase activity of yHSP90α$^{\Delta(211\text{-}259)}$ was reduced by 2.5-fold, although that of yHSP90α$^{\Delta(211\text{-}242)}$ showed a similar fold stimulation as that of the wild-type yHSP90α. One of the CL mutants was characterized in detail for its role in DNA repair pathway. It was reported that although the stability of Rad51 remains unaffected in the *hsp82(Δ211-259)* mutant, the strain displays a severe reduction in the gene targeting efficiency (Suhane *et al.*, 2014). Moreover, the MMS-induced Rad51 foci formation, which is the hallmark of HR-mediated DNA repair, was significantly reduced in this mutant background. However, the mechanism behind such phenotype is not understood well.

A recent study in mammalian systems shows that DNA-PK-mediated Thr7 phosphorylation of HsHSP90α in response to DNA damage causes its recruitment to the DSBs (Quanz *et al.*, 2012). In a separate study it has been demonstrated that exposure to ionizing radiation causes the phosphorylation of Thr5/Thr7 residues of the nuclear pool of Hsp90 by ataxia telangiectasia mutated (ATM) kinase and this is vital for the maintenance of γH2AX levels (Elaimy *et al.,* 2016). In lower eukaryotes such as in budding yeast, yHSP90α neither possesses the first 14 stretch of amino acids, including the Thr5 and Thr7 residues, nor harbors DNA-PK. Furthermore, although the orthologs of ATM, i.e., Tel1/Mec1 are present in yeast, there is no report showing their physical association with yHSP90α. This raises the question of whether DNA damage-induced chromatin recruitment of HSP90α occurs in these organisms. Furthermore, it was never addressed whether cellular redistribution of yHSP90α occurs in response to DNA damage and whether phosphorylation of Thr5/Thr7 of HsHSP90α is a prerequisite for the nuclear import. Also, it remains unanswered whether the nuclear function of HSP90α is essential for HR-mediated DSB repair pathway.

In our present study, we have addressed all the above-mentioned questions and identified a novel pathway for DNA damage-induced nuclear translocation of yHSP90α. We have discovered that Aha1 regulates the nuclear import of yHSP90α. To better understand the function of yHSP90α in HR-mediated DNA repair pathway, we have used chromatin immune precipitation assay to investigate the association of yHSP90α and Rad51 with damaged DNA after we artificially induce the DSB. Concurrently, the repair kinetics of the damaged DNA were analyzed. The combined results of these two approaches enabled us to compare the extent of occupancy of yHSP90α and Rad51 with the DSB ends and its flanking regions. In a HR-defective CL-deleted yHSP90α mutant strain (Suhane *et al.*, 2014), we observed a defect in the nuclear import and chromatin association of the Hsp90$^{\Delta(211\text{-}259)}$ protein. Collectively, Aha1 appears to play a critical role in the nuclear import of yHSP90α, which in turn is vital for HR-mediated DNA repair pathway. This is supported by the sensitivity of Δ*aha1* strain toward different genotoxic agents.

RESULTS

Accumulation of yHSP90α in the nucleus in response to MMS-induced DNA damage

It was reported earlier that upon DNA damage, human HSP90α is phosphorylated by DNA-PK at threonine 5/7 residues and that the phosphorylated form of HsHSP90α is accumulated at the site of DNA damage (Quanz *et al.*, 2012; Elaimy *et al.*, 2016). Although DNA-PK can phosphorylate both the cytoplasmic and the nuclear pool of HsHSP90α upon DNA damage, it was never addressed whether there is a DNA damage-induced upsurge of HSP90α in the nucleus and whether this import is dependent on the threonine 5/7 phosphorylation. We investigated whether the nuclear translocation of yHSP90α occurs in an aforementioned phosphorylation-independent manner in *S. cerevisiae*, in which the first 14 amino acids are absent (Supplemental Figure S1, red circle). Earlier we observed that the association between Rad51 and yHSP90α was reduced in the presence of MMS (0.15%); hence we used the same dose of MMS for our present study (Suhane *et al.*, 2019). We examined the level of yHSP90α in whole-cell extract and in nuclear fraction of W303a strain upon exposure to MMS treatment (0.15%). We found that there was no difference in the expression of yHSP90α in response to DNA damage (Figure 1A, left panel); however, it was redistributed to the nucleus (Figure 1A, right panel). The experiment was repeated more than three times and one set of the representative Western blot images is presented. Rad51 level was monitored as a positive control which showed more than two- and threefold of induction in the whole-cell extract and in the nuclear fraction, respectively (Figure 1B). The nuclear fractionation data showed that upon MMS treatment, there was a 2.5-fold nuclear enrichment of yHSP90α (Figure 1B). Nsp1, the nuclear marker protein, was used as a loading control. The nuclear accumulation of yHSP90α was further supported by the live-cell imaging of the strain *NFY31* that harbors a single-copy GFP fused yHSP90α plasmid. We observed that in the untreated condition, GFP-yHSP90α was uniformly distributed throughout the

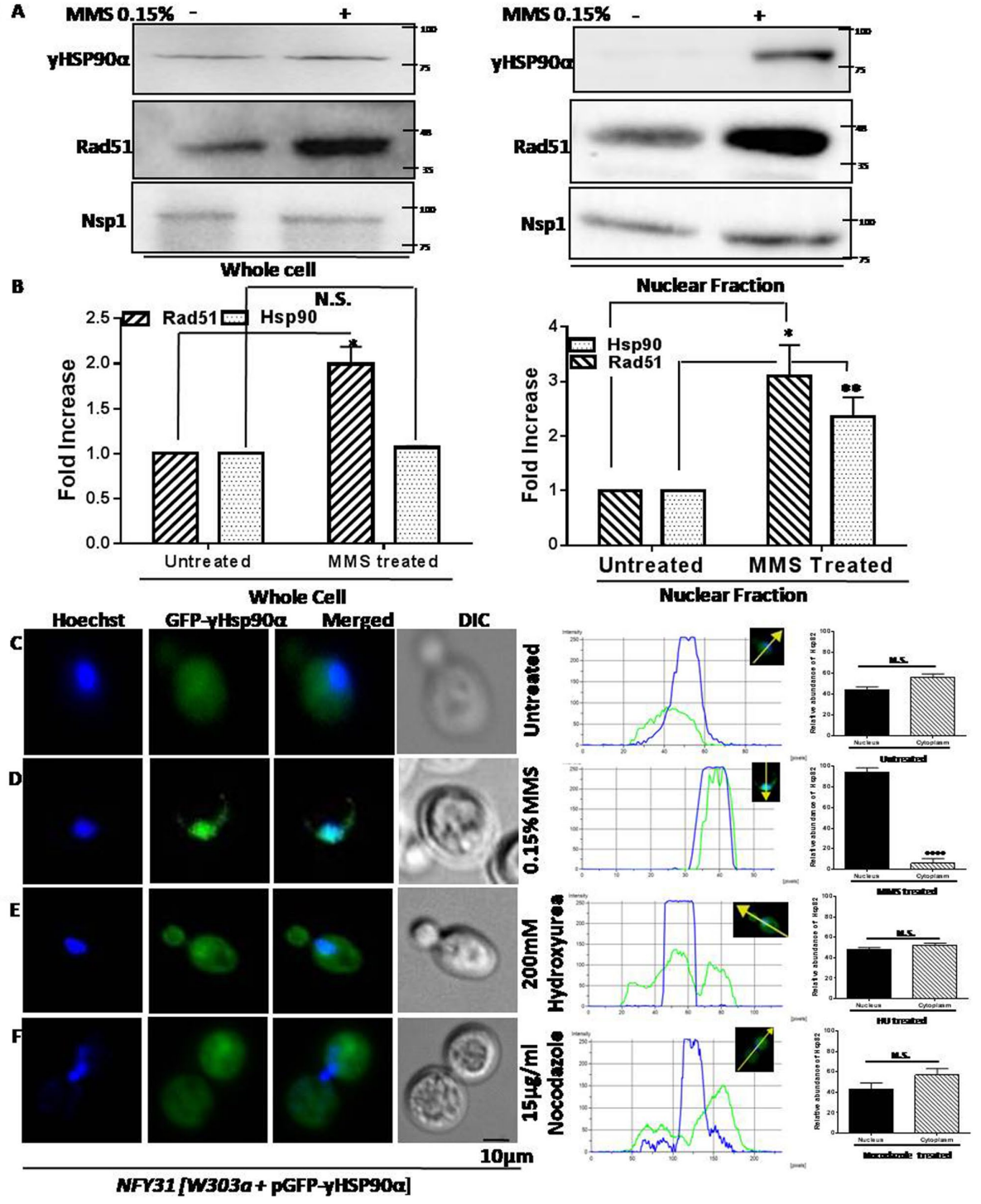

FIGURE 1: Accumulation of yHSP90α in the nucleus in response to MMS-induced DNA damage. (A) Western blots showing no difference in the steady state expression of yHSP90α in the whole cell with (+) and without (–) MMS treatment (left panel). yHSP90α was accumulated in the nuclear fraction upon MMS treatment (right panel); Rad51 acted as a positive control for MMS treatment; Nsp1 acted as a nuclear marker. (B) The above experiment was repeated three times, and the mean values (±SD) were plotted. *P* values were calculated using the two-tailed Student's *t* test (***P* < 0.01; **P* < 0.05). (C) Live-cell imaging shows the distribution of GFP-yHsp90α (green) in the whole cell in the untreated condition. (D) Fluorescence imaging of 0.15% MMS-treated cells shows the localization of GFP-yHsp90α (green) inside the nucleus (blue). (E) Fluorescence images showing no nuclear accumulation of GFP-yHsp90α (green) in 200 mM hydroxyurea-arrested early S phase cells (F) Fluorescence images showing no nuclear accumulation of GFP-yHsp90α (green) in 15 µg/ml nocodazole-arrested G2/M cells. Nucleus was stained using Hoechst 33342. Intensity profiles were derived for all fluorescence experiments using NIS elements AR software; the relative fluorescence intensities of GFP-yHsp90α in the nucleus and cytoplasm were quantified and the mean values (±SD) were plotted using GraphPad Prism 6. *P* values were calculated using the two-tailed Student's *t* test (*****P* < 0.0001; N.S., not significant).

cell (Figure 1C). However, when treated with 0.15% MMS, GFP-yHSP90α moved to the nucleus and coincided with Hoechst 33342 (Figure 1D). As MMS delays S-phase progression, we wanted to distinguish whether the nuclear translocation of yHSP90α occurs as a consequence of cell cycle arrest or as a consequence of DNA damage. For that, we used hydroxyurea-induced S-phase-arrested cells and the nocodazole-induced G2/M-arrested cells and looked for the distribution of GFP-yHsp90α. We found that GFP fluorescence was distributed majorly in the cytoplasm and to a little extent in the nucleus of the hydroxyurea-arrested cells (Figure 1E). We also found that GFP-yHsp90α was evenly distributed throughout the cytoplasm in the nocodazole-arrested cells (Figure 1F) and didn't coincide with the blue fluorescence of Hoechst. Thus our study concludes that nuclear redistribution of yHsp90α is associated with MMS-induced DNA damage. We further examined whether human HsHSP90α shows similar localization dynamics in response to MMS treatment. We used the strain harboring a plasmid that expresses human HSP90α fused with FLAG. We verified that FLAG antibody does not show any cross-reactivity with other yeast proteins (Supplemental Figure S2A). The nuclear fractionations showed increased levels of HsHSP90α in the MMS-treated sample compared with the untreated sample (Figure 2A). Quantification of gel images from an independent set of experiments showed about a fourfold increase in the HsHSP90α level within the nucleus (Figure 2B). We sought to determine whether this import is dependent on the presence of Thr 7 residue of HsHSP90α. Using a mutant protein HsHSP90α^{T7A}, where threonine is mutated to alanine, we observed that its nuclear import remained unperturbed (Figure 2C). Estimation of multiple WBs showed about a fivefold increase in the nuclear fraction with respect to the untreated cell (Figure 2D). Thus our study shows that DNA damage induces an increased import of HSP90α in the nucleus from the cytoplasm which is independent of phosphorylation of the threonine 7 residues.

Nuclear accumulation of yHSP90α upon induction of a single double-strand break

MMS alkylates DNA bases and thereby causes DNA-base mispairing (Lundin *et al.*, 2005). To understand whether the increased nuclear yHSP90α reflects a true response to DNA damage, we induced a single double-strand break in DNA and determined the cellular redistribution of yHSP90α. To that end, we used the *NA14* strain (Agmon *et al.*, 2009), where a site-specific DSB was created within the mutant *ura3* locus by expressing a galactose-inducible *HO* endonuclease (Figure 3A). By designing the primers complementary to the region adjacent of the *HOcs* (OSB 289) and the regions within the *KANMX* cassette (kanB1), we measured the extent of DNA cleavage by the HO endonuclease. We have repeated the repair kinetics upon *HO* induction with three independent batch of cells and one of the representative images is provided (Figure 3B). We found that the *HO* endonuclease resulted in 75% cleavage at the *ura3* locus within the first hour of induction and 100% by the end of the second hour (Figure 3C). The DSBs are repaired by HR using a donor *URA3* sequence that is placed 3 kb apart. We observed that 50% repair was achieved at the end of the third hour and the damage was completely healed by the end of the fourth hour (Figure 3, B and C). As in our experimental setup, we always observed maximum damage at the second hour of galactose induction (Figure 3C), we harvested the cells before and at the second hour after the galactose treatment, and performed the nuclear fractionation. We observed that there was no difference in the expression of yHSP90α in the whole cell and at the second hour postinduction, the protein showed significant nuclear enrichment upon formation of a single

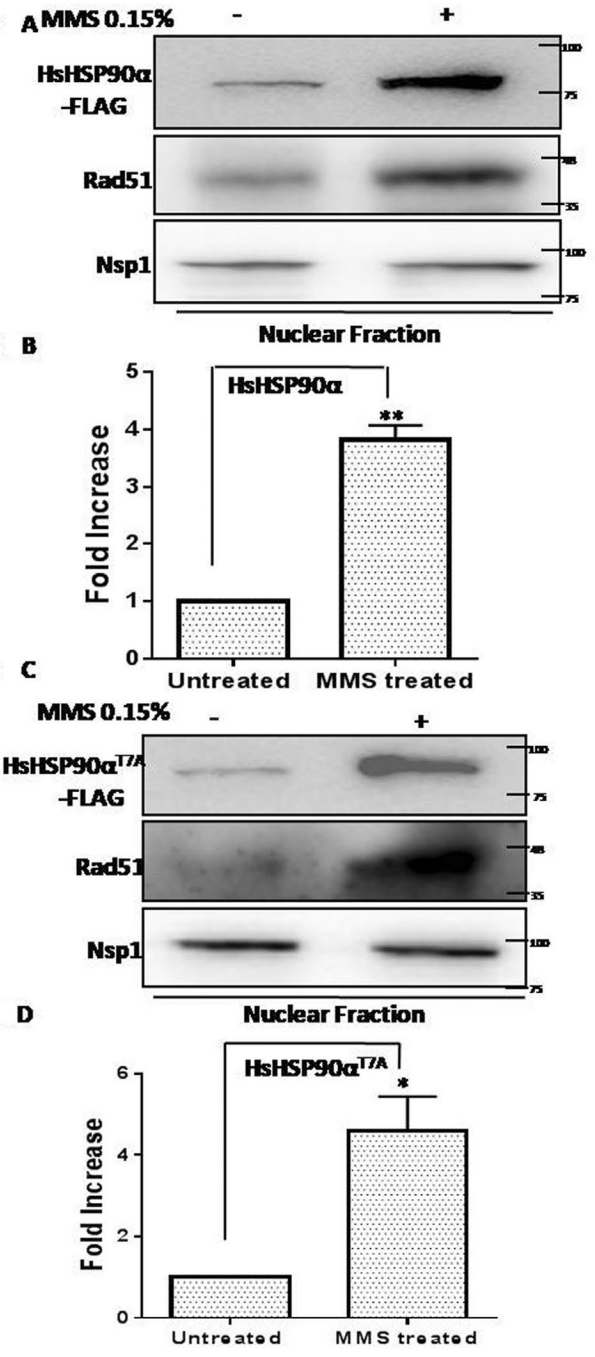

FIGURE 2: Accumulation of HsHSP90α in the nucleus in response to MMS-induced DNA damage. (A) Western blot showing the nuclear fractionation of *FLAG* tagged *HsHSP90α* strain in the presence and absence of MMS treatment. (B) The experiment was repeated with a fresh batch of cells and estimation of band intensities showed a fourfold increase in the nuclear accumulation of HsHSP90α in the presence of MMS. (C) Western blot showing the results of nuclear fractionation of *FLAG* tagged *Hshsp90αT7A* strain in the presence and absence of MMS treatment. (D) Quantification of band intensities of independent experiments showed a fivefold increase in the nuclear distribution of the mutant protein; *P* values were calculated using the two-tailed Student's *t* test (**$P < 0.01$; *$P < 0.05$).

DSB in chromosome (Figure 3D). Quantification of the independent WB image showed about a fourfold increase in the nuclear level of yHSP90α at 2 h post-HO induction (Figure 3E). Hence we observe

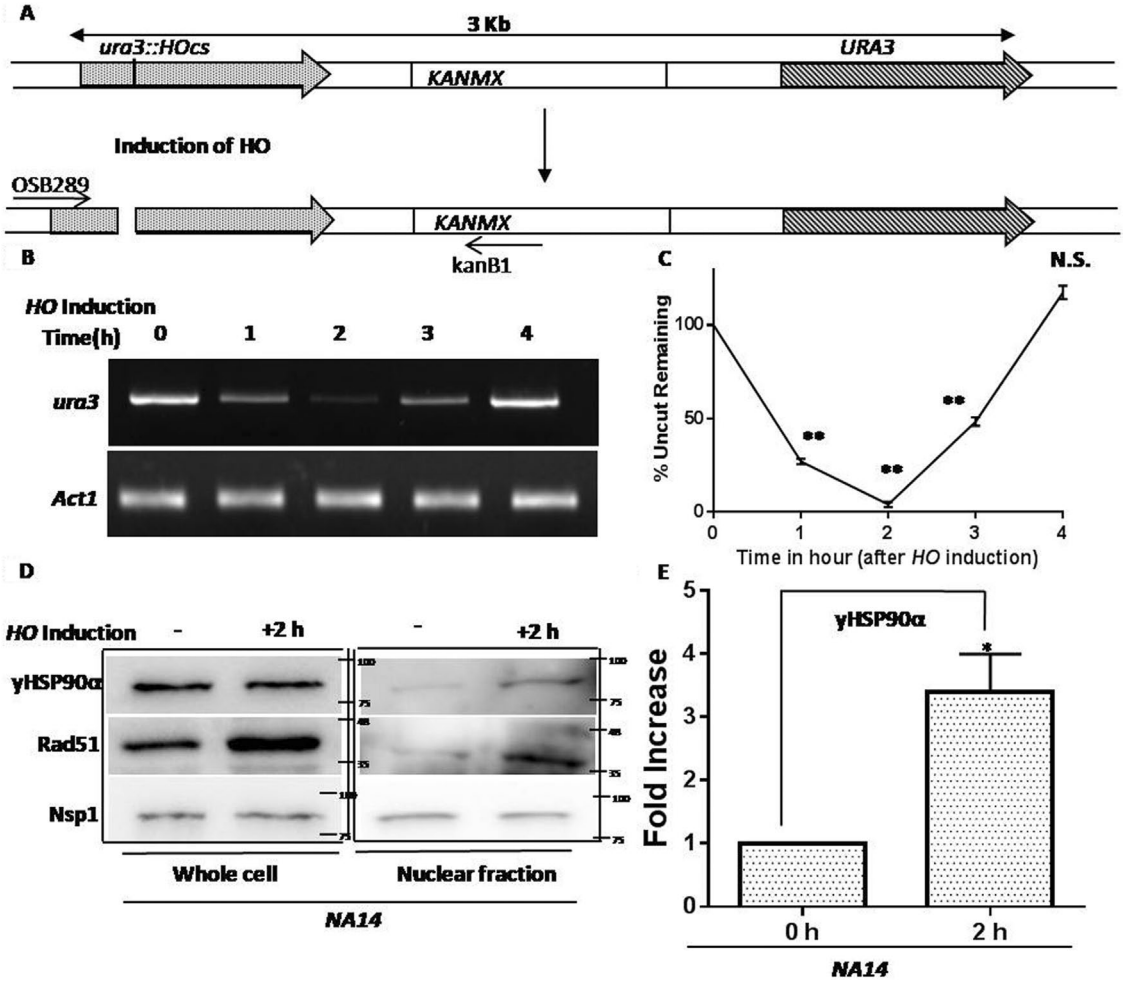

FIGURE 3: Nuclear accumulation of yHSP90α upon induction of a single double-strand break. (A) Schematic representation of the cassette incorporated in the *NA14* strain in which two homologous *URA3* sequences are separated by 3-kb intervals on chromosome V with the sequence of *KANMX* integrated in between. One of the *URA3* sequences has *HO* endonuclease recognition site (HOcs) incorporated in it. The relative positions of the primer pairs OSB289 and KanB1 were shown, which were used to detect the DNA damage upon *HO* induction. (B) *NA14* cells were grown and *HO* induction was done by growing cells in galactose medium. Genomic DNA was extracted at different time intervals (0 to 4 h) and subsequently amplified using the primer pairs OSB289 and KanB1, where the absence of band indicated DNA damage. DNA levels were normalized with respect to *ACT1*. (C) The above experiment was repeated with three independent batches of cells and the mean values (±SD) were plotted. The repair kinetics showed maximum damage at the second hour of *HO* induction and complete repair was seen at the fourth hour of induction. The mean values (±SD) were plotted; the significance was calculated with respect to the untreated sample (0 h); *P* values were calculated using the two-tailed Student's *t* test (***P* < 0.01, NS, not significant). (D) The steady state levels of yHSP90α in *NA14* strain were presented at 2 h before (–) and after (+) *HO* induction (left panel). In the same conditions, nuclear fractionations were done which showed increased nuclear accumulation of yHSP90α at the second hour of induction (right panel). Rad51 up-regulation served as a control for DSB; protein levels were normalized with respect to Nsp1. (E) Quantification of yHSP90α levels as obtained from independent set of experiment showed fourfold increase at 2 h post-*HO* induction. The mean values (±SD) were plotted, *P* values were calculated using the two-tailed Student's *t* test (**P* < 0.05).

that even a single DSB in chromosome causes an increased nuclear accumulation of yHSP90α.

Kinetics and extent of occupancy of yHSP90α at DSB ends

In mammalian cells it was demonstrated that DNA damage-induced T7-phosphorylated form of HsHSP90α is recruited to the damaged chromatin. However, whether this phosphorylation is a criterion for its chromatin recruitment was not addressed. In *S. cerevisiae* yHSP90α lacks the stretch of 14 residues, including T7 of HsHSP90α. We wanted to check whether the nuclear pool of yHSP90α was associated with the damaged chromatin. We utilized the chromatin immunoprecipitation technique to visualize the kinetics and extent of yHSP90α binding following DSB induction and during its repair by HR. In *NA14* yeast cells, the DSB created at the *ura3* locus can be repaired by HR using a donor template (*URA3*) that is located 3 kb apart (Figure 4A). To monitor yHSP90α binding to DSB ends, we performed ChIP analysis immediately after *HO* induction and at every 1-h interval up to 4 h (the time required for its complete repair). Significant yHSP90α binding to sequences close to the *HO* cleavage site was observed at the second and third hours using a pair of primers (shown as horizontal bars), OSB 519 and OSB 520, that amplify sequences 55 to 205 bp proximal to the *HO* cut site (Figure 4B).

There was no association of yHSP90α to other locus (*ACT1*). The maximum recruitment of yHSP90α to DSB was observed at the second hour. It is noteworthy that the maximum break was generated during the second hour post-HO treatment and by the third hour 50% break was repaired (Figure 3C). Thus the entry and exit of Hsp90 correlated well with the presence of maximum break as seen in Figure 3B and it remained associated up to the third hour until 50% of the DSB remained unrepaired (Figure 3C). At a later time point (the fourth hour), the recruitment was substantially reduced. As a reference, we monitored the recruitment of Rad51 under similar conditions and observed a slightly different pattern (Figure 4C). We calculated the fraction of recruitment of yHSP90α and Rad51 and plotted against different time intervals. We found that yHSP90α recruitment was highest at the time of maximum damage (second hour) and it was dislodged from the chromatin at the fourth hour of *HO* induction once repair was complete (Figure 4D). Rad51 recruitment had been initiated at the second hour, which remained maximum at the third hour and a significant amount of Rad51 remained associated even at the fourth hour (Figure 4D). We also measured the association of yHSP90α and Rad51, at the leftward direction (up to 5 kb) from the cleavage sites. We found a similar pattern, i.e., significant recruitment of yHSP90α and Rad51 was observed throughout 4 kb regions during the second and third hours post-*HO* induction (Figure 4E). Thus our study has established that a DNA damage-induced increase in association of yHSP90α to the chromatin is independent of the N-terminal 14-residues present in HsHSP90α.

Increased nuclear localization of Aha1 in response to DNA damage

We further investigated DNA damage-induced nuclear accumulation of the Hsp90 cochaperone Aha1. We employed indirect immunofluorescence to monitor the cellular localization of Aha1 in *W303a* strain. We observed that Aha1 was equally distributed in the nucleus and in the cytoplasm before (Figure 5A) and after MMS treatment (Figure 5B). However, there was an overall increase in the Aha1 fluorescence intensity in the cell in response to MMS (Figure 5B). Such induction corroborated well with our Western data with the whole cell, where we found that endogenous level of Aha1 was significantly induced upon MMS treatment (Figure 5C, left panel). We also observe a concomitant increase in the Aha1 level in the nucleus (Figure 5C, right panel) upon MMS treatment. It is noteworthy that Aha1 antibody used in this study is highly specific and does not cross-react with any other proteins in WB and does not give any background in IFA (Supplemental Figure S2D). We wanted to determine whether induction of a single double-strand break in the chromosome could also induce the import of Aha1 to the nucleus. For that, we used the NA14 strain. Our results showed that in this strain, the Aha1 protein level in the nucleus was significantly increased, about 1.5-fold, at the second hour of *HO* induction (Figure 5, D and E), whereas the yHSP90α level was increased about threefold. We also monitored whether Aha1 was also recruited to DSB ends like yHSP90α. However, we could not detect Aha1 in the ChIP assay (data not shown). We speculate that Aha1 may be transiently associated to chromatin, which could not be detected in our assay. Next, to investigate whether other cochaperones such as Sba1 and Cdc37 are imported to the nucleus upon DNA damage, we used carboxy-terminal *MYC* tagged Sba1 and Cdc37 strains for our analysis. We found that there was no such increase in the levels for Cdc37 in the whole cell as well as in the nucleus upon DNA damage (Figure 5F). In the case of Sba1, we found that its endogenous level was significantly induced upon MMS treatment similar to that of Aha1 (Figure 5G, left panel). However, unlike Aha1, there was no such increase in Sba1 level in the nucleus (Figure 5G, right panel). We have repeated these experiments three times and the nuclear distribution of each of the cochaperones was plotted in the presence and absence of MMS. It was found that in the whole-cell extract, the abundance of Aha1 and Sba1 was threefold and fourfold, respectively (Figure 5H); however, only Aha1 showed about a twofold increased accumulation in the nucleus upon MMS treatment, while Sba1 and Cdc37 showed no significant increase (Figure 5I). To address whether MMS-induced up-regulation of Aha1 and Sba1 occurs at the transcription level, we compared the relative expression of the above-mentioned cochaperones in the absence and presence of 0.15% MMS (Supplemental Figure S3A). Quantitative reverse transcription PCR (RT-PCR) shows a 1.5-fold increase in expression of *AHA1* and no significant increase in expression of *SBA1* upon MMS treatment (Supplemental Figure S3B). An increase in *RAD51* transcript was used as a positive control in our study. We speculate that the higher abundance of *SBA1* may result due to increased protein stability during genotoxic stress.

yHsp90α transport to the nucleus upon DNA damage is independent of Cdc37 and Sba1

Next, we wanted to address whether DNA damage-dependent increased nuclear accumulation of yHSP90α is dependent on Cdc37 and Sba1. We used the temperature-sensitive *cdc37S14A* mutant strain, which shows normal phenotype at 25°C but displays a complete loss of function when grown at a restrictive temperature 37°C. Our study showed no difference in the endogenous level of yHSP90α in the *cdc37S14A* mutant strain when grown at 37°C in the presence or absence of MMS (Figure 6A). The nuclear fractionation under similar conditions showed a fourfold increase in the accumulation of yHSP90α upon DNA damage (Figure 6, B and C), similar to that observed in the wild-type strain. To address the dependency on Sba1, we generated a Δ*sba1* strain in an isogenic *W303a* background. We found that in the Δ*sba1* strain, the yHSP90α level was induced by 3.6-fold in the whole cell in response to MMS treatment (Figure 6, D and F). In addition, DNA damage-dependent nuclear import was observed in a manner nearly indistinguishable from the wild-type cells (Figure 6, E and F). Together, this study concludes that MMS-induced nuclear import of yHSP90α is independent of Cdc37 and Sba1.

yHSP90α transport to the nucleus upon DNA damage is dependent on Aha1

To decipher whether Aha1 plays any role during MMS-induced nuclear import of yHSP90α, we generated Δ*aha1* strain. We transformed empty plasmid and *AHA1* overexpression plasmid to Δ*aha1* strain to generate two isogenic strains. *AHA1* expression was detected specifically in Δ*aha1* strain harboring the *AHA1* overexpression plasmid (Figure 7A, third lane). Interestingly, we found that Aha1 deletion was positively correlated with MMS-induced up-regulation of endogenous yHSP90α (Figure 7A), and the phenotype is reversed with ectopic expression of *AHA1* as presented in Figure 7A (first lane). Further, we observed that although Aha1 deletion resulted in a 3.5-fold induction in the endogenous level of yHSP90α upon MMS treatment (Figure 7B), it couldn't be translocated to the nucleus (Figure 7C, first lane). However, ectopic expression of Aha1 resulted in the increased nuclear import of both yHSP90α (approximately threefold) and Aha1 upon DNA damage (Figure 7, C and D). We used live-cell fluorescence to visualize the localization of yHSP90α in the Δ*aha1* strain *NFY32* that harbors a centromeric GFP-yHSP90α plasmid. We didn't find any nuclear localization of yHSP90α under the MMS-treated (Figure 7, F and G) or untreated (Figure 7, E and G) condition. This experiment was

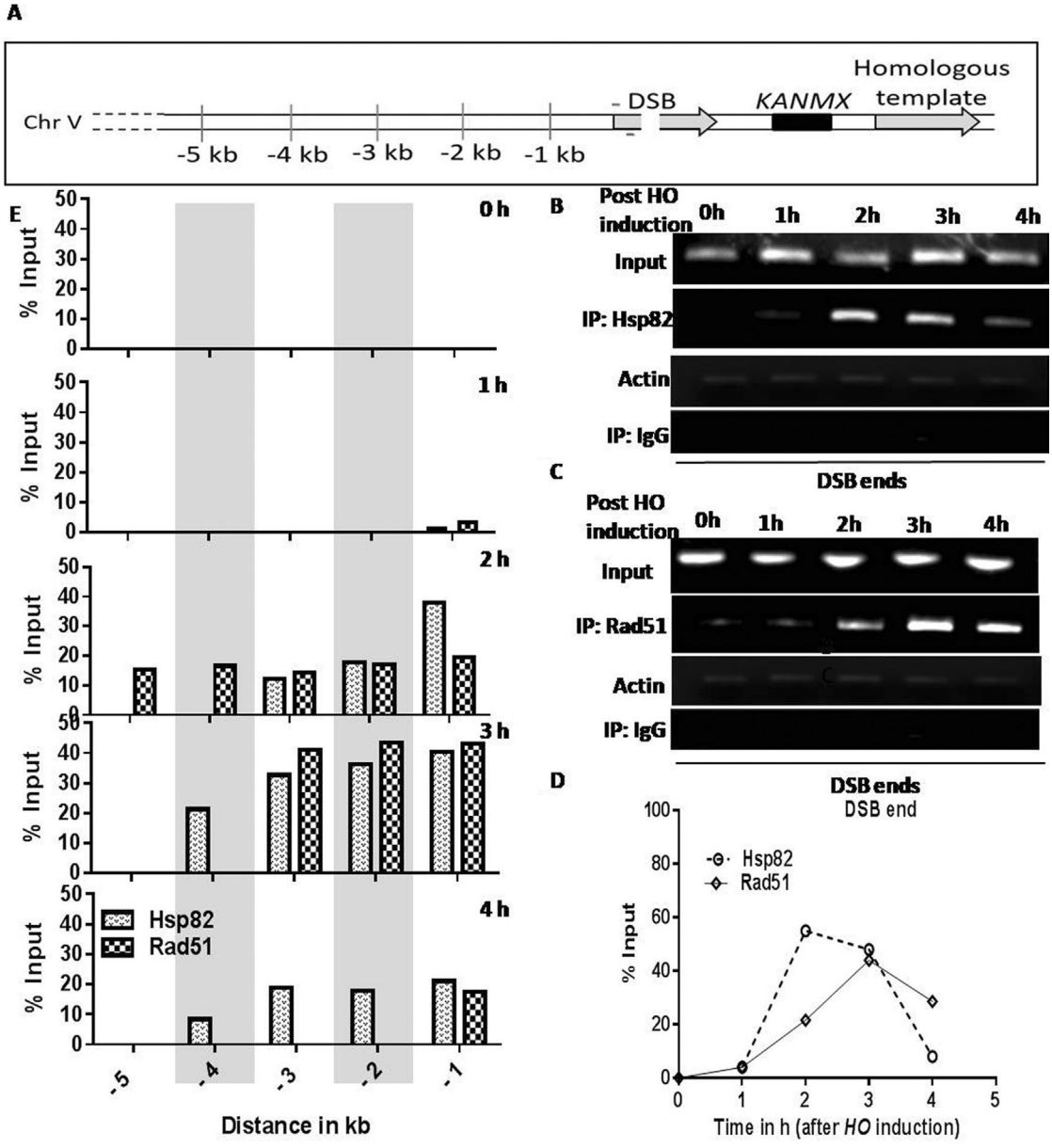

FIGURE 4: Kinetics and extent of occupancy of yHSP90α at DSB ends. (A) Schematic representation of the position of DSB at the *ura3* locus and the presence of a homologous template (*URA3*). The position of the primers (as indicated in horizontal bar) near the DSB was presented, which was used to detect the recruitment of yHSP90α and Rad51 near the *HO* cleavage site. The map of the sites (up to - 5 kb) distal to the DSB was shown. (B) yHSP90α bound chromatin was amplified to detect the kinetics of its recruitment to the *HO* cleavage site and at the *ACT1* locus. (C) ChIP analysis showing the kinetics of Rad51 recruitment to the DSB ends as well as at the *ACT1* locus following *HO* induction. (D) Quantification of the independent ChIP experiments ($n = 3$, in each case) was plotted. Error bars indicated SD. (E) The association of yHSP90α and Rad51 was measured at increasing distances up to 5 kb upstream of the *HO* cleavage site at different time points post-*HO* induction. Quantification of two independent ChIP experiments were plotted to compare the extent of recruitment between yHSP90α and Rad51. Error bars indicated SD. ChIP assay was done with IgG antibody that was used as a negative control.

performed along with its isogenic control strain (Figure 1, C and D). To understand whether yHSP90α and Aha1 remain associated under the MMS-treated condition, we performed coimmunoprecipitation study. We used a strain KRAY29, that harbors a plasmid with C-terminal FLAG tagged Aha1. Aha1 was pulled down with anti-FLAG antibody in MMS-treated and untreated conditions and we looked for the presence of yHSP90α in the IP fraction. We found that Aha1 and yHSP90α remained physically associated in both the conditions (Figure 7H).

To understand whether the Aha1-dependent nuclear import of yHSP90α is a generalized phenomenon in budding yeasts, we used another Δ*aha1* strain in the *BY4741* background and wanted to test the same in this strain background. In *BY4741* whole-cell extract, where Aha1 protein was completely absent (Figure 8A, left panel), we found similar up-regulation of yHSP90α in response to MMS. However, we find complete abrogation of the nuclear accumulation of yHSP90α (Figure 8A, right panel). We loaded a higher amount of protein in the MMS-treated condition compared with the other

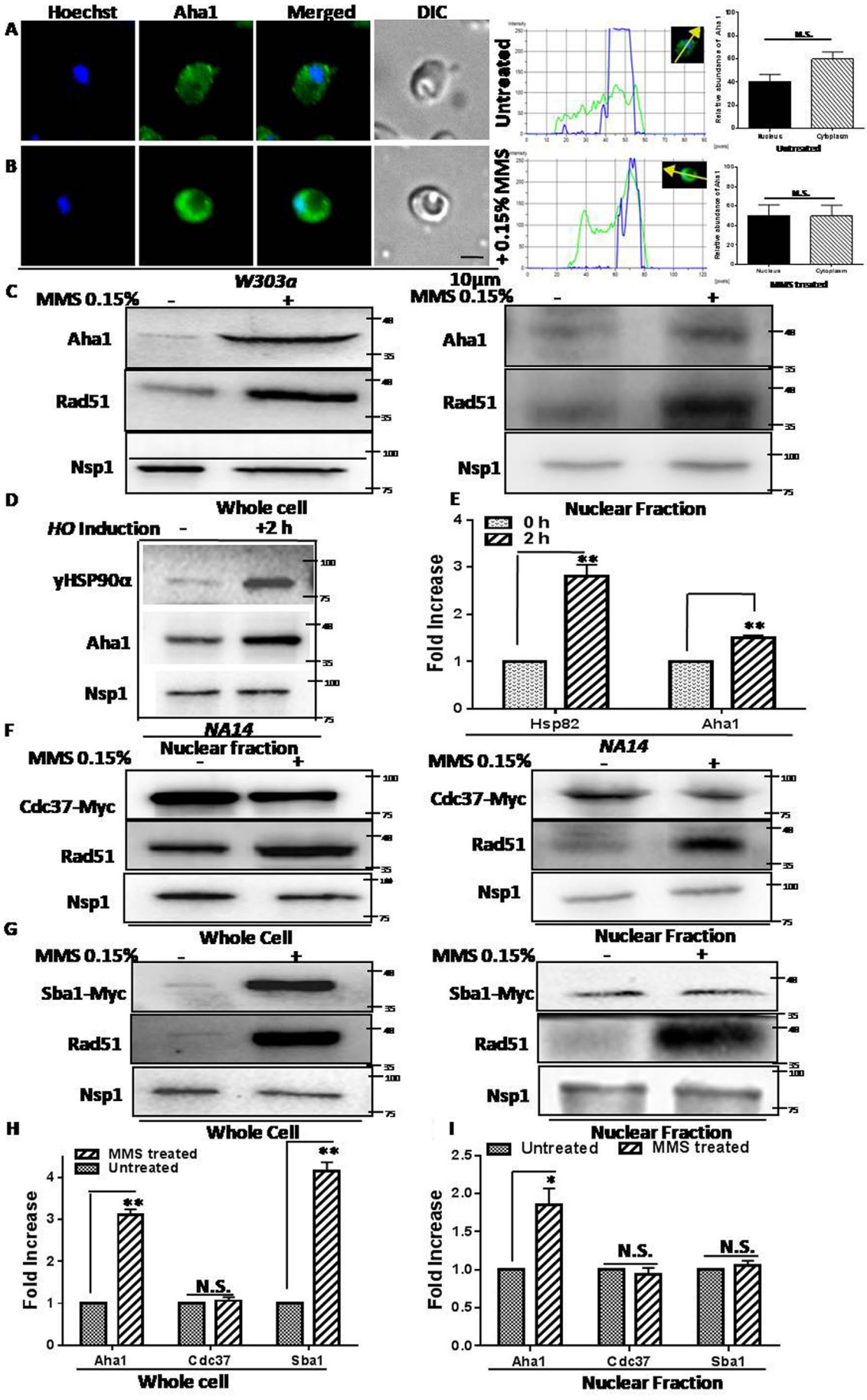
A
Hoechst
Aha1
Merged
DIC
Untreated
N.S.
Relative abundance of Aha1
Nucleus
Cytoplasm
Untreated
B
+0.15% MMS
N.S.
Nucleus
Cytoplasm
MMS treated
C
W303a
MMS 0.15%
Aha1
Rad51
Nsp1
Whole cell
10µm
MMS 0.15%
Aha1
Rad51
Nsp1
Nuclear Fraction
D
HO Induction
+2 h
yHSP90α
Aha1
Nsp1
E
0 h
2 h
Fold Increase
Hsp82
Aha1
F
NA14
Nuclear fraction
MMS 0.15%
Cdc37-Myc
Rad51
Nsp1
Whole Cell
NA14
MMS 0.15%
Cdc37-Myc
Rad51
Nsp1
Nuclear Fraction
G
MMS 0.15%
Sba1-Myc
Rad51
Nsp1
Whole Cell
MMS 0.15%
Sba1-Myc
Rad51
Nsp1
Nuclear Fraction
H
MMS treated
Untreated
Fold Increase
N.S.
Aha1
Cdc37
Sba1
Whole cell
I
Untreated
MMS treated
Fold Increase
N.S.
N.S.
Aha1
Cdc37
Sba1
Nuclear Fraction

lanes as seen by the amount of Nsp1 (Figure 8A, right panel, last lane); however, there was no signal of yHSP90α in the nuclear fraction. We overexpressed *AHA1* in the *BY4741Δaha1* strain and performed the nuclear fractionation in the presence and absence of MMS. The Western blot of the whole-cell extract showed no change in the endogenous level of yHSP90α in the presence and absence of MMS (Figure 8B, left panel). However, the presence of Aha1 promoted the nuclear import of yHSP90α in a MMS-dependent manner (Figure 8B, right panel). Together, our data establish that the presence of Aha1 is essential for the nuclear localization of yHSP90α.

The domain responsible for the conformational flexibility between the amino terminal and the MD of yHSP90α is essential for its nuclear translocation upon DNA damage

It was earlier established that the conformational flexibility between the amino terminal domain and the MD of yHSP90α is mediated by a flexible CL domain spanning 211-259 residues, as presented in the schematic diagram (Figure 9A). The deletion of these highly charged amino acid stretches (211-259) leads to a significant reduction in Aha1-stimulated ATP hydrolysis of yHSP90α (Hainzl *et al.*, 2009). However, deletion of a shorter stretch (211-242) does not alter the conformational flexibility of the mutant protein and it shows comparable Aha1-mediated ATPase activation of yHSP90α as that of the wild-type protein (Hainzl *et al.*, 2009). We wanted to determine whether this domain known for providing conformational flexibility between the amino-terminal and the middle domain is important for its nuclear import. We investigated the MMS-induced nuclear import of the two mutant proteins yHSP90α$^{\Delta(211\text{-}259)}$ and yHSP90α$^{\Delta(211\text{-}242)}$ using live-cell fluorescence imaging. For that, we generated NFY33 and NFY35 strains that harbor a centromeric plasmid expressing GFP-yHSP90α$^{\Delta(211\text{-}259)}$ and GFP-yHSP90α$^{\Delta(211\text{-}242)}$, respectively. We observe that in the GFP-yHSP90α$^{\Delta(211\text{-}259)}$ harboring strain, GFP fluorescence does not merge with Hoechst fluorescence in the presence (Figure 9C) as well as the absence of MMS (Figure 9B). However, there is a distinct nuclear accumulation in the case of the shorter deletion mutant GFP-yHSP90α$^{\Delta(211\text{-}242)}$ upon MMS treatment (Figure 9, D and E). A representative image from each sample is presented. To confirm the result by an alternate method, we isolated the nuclear fraction from the previously characterized CL deletion strain (Louvion *et al.*, 1996) which was shown to be severely defective in HR activity (Suhane *et al.*, 2014). We observed a complete absence of the mutant protein yHSP90α$^{\Delta(211\text{-}259)}$ in the nucleus of the MMS-treated cell (Figure 10A, right panel). We loaded a higher amount of the mutant protein compared with the wild-type as seen by the level of Nsp1 (last lane, Figure 10A, right panel) but could not detect the protein in the nucleus. The Western blot analysis of the whole-cell extracts with the mutant strain confirmed the expression of the mutant protein (Figure 10A, left panel). To test whether Aha1 overexpression can promote the MMS-induced nuclear import of the longer CL deletion mutant, we transformed the *AHA1* overexpression plasmid in the *hsp82Δs211-259)* strain. We found that *AHA1* overexpression did not impact the translocation of the mutant protein to the nucleus (Figure 10B, right panel). It was previously shown that the CL region of human HSP90α provides flexibility for domain rearrangements and acts as a modulator of chaperone activity (Tsutsumi *et al.*, 2012). We wanted to determine whether the deletion of identical stretch of charged residues from human HSP90α causes a similar defect. To that end, we have generated a strain harboring human HsHSP90α$^{\Delta(224\text{-}279)}$, still expressing endogenous yHSP90α (Supplemental Figure S1). The mutant protein showed expression as presented (Supplemental Figure S2B). We found that the mutant human protein did not show (Figure 10C) any increased nuclear accumulation upon DNA damage. The level of yHSP90α was increased in the nucleus under such conditions (third panel, Figure 10C). It is noteworthy that the antibody recognizing HsHSP90α (anti-FLAG) does not recognize yHSP90α (Supplemental Figure S2B). Next, we performed the nuclear fractionation to detect the level of the shorter CL deletion mutant yHSP90α$^{\Delta(211\text{-}242)}$ upon MMS treatment. For that, we created a strain *KRAY16* in which the endogenous *Hsp82* and *Hsc82* are knocked out and the strain expresses yHSP90$^{\Delta(211\text{-}242)}$ from a single copy plasmid. We observed that the mutant protein is accumulated to the nucleus in response to MMS treatment, correlating our live-cell imaging data (Figure 10D). The experiment was repeated three times and the estimation of band intensities showed about a fourfold increase in the nuclear level of the mutant yHSP90α$^{\Delta(211\text{-}242)}$ in this strain background (Figure 10E). Taken together, we conclude that the CL domain of HSP90α is essential for its import to the nucleus. To support our conclusion further, we measured the single DSB-induced chromatin recruitment of the mutant yHSP90α$^{\Delta(211\text{-}259)}$. To that end, we generated a modified *NA14* strain which harbors a plasmid that expressed the mutant yHSP90α$^{\Delta(211\text{-}259)}$ fused with GFP at its amino terminal end. The isogenic strain was generated which harbors wild-type GFP-yHSP90α- constructs, and both the fusion proteins were found to be

FIGURE 5: Increased nuclear localization of Aha1 in response to DNA damage. (A) Indirect immunofluorescence shows the distribution of Aha1 (green) in the whole cell of W303a (B) A part of Aha1 fluorescence (green) merges with the Hoechst fluorescence (blue) in the MMS-treated condition, although at is distributed in the cytoplasm as well. Nuclear staining was done using Hoechst dye and Aha1 was detected using Alexa Fluor 488–conjugated secondary antibodies. Intensity profiles were derived for all fluorescence experiments using NIS elements AR software; relative fluorescence intensities of Aha1 in the nucleus and cytoplasm were quantified and the mean values (±SD) were plotted using GraphPad Prism. *P* values were calculated using the two-tailed Student's *t* test (N.S., not significant). (C) Aha1 is induced in the whole cell (left panel) in the presence of MMS and its level in the nucleus in increased (right panel) in response to 0.15% MMS treatment. (D) *NA14* strain was subjected to *HO* induction in the same manner as discussed in Figure 3. The experiment was repeated and one of the representative Western blots was presented. (E) Quantification of the levels of yHSP90α and Aha1 showed threefold and 1.5-fold increased nuclear accumulation, respectively, at 2 h post-*HO* induction. The mean values (±SD) were plotted. *P* values were calculated using the two-tailed Student's *t* test (***P* < 0.01). (F) Cdc37 level is not altered significantly upon 0.15% MMS treatment in the whole cell (left panel) as well as in the nucleus (right panel). (G) Sba1 is induced in the whole cell (left panel) in response to 0.15% MMS; however, nuclear fractionation shows no change in nuclear level of Sba1 in the presence and absence of MMS (right panel). (H) and (I) The experiments in C, F, and G were repeated with an independent batch of cells and the quantitation of the data was done using ImageJ and mean values (±SD) were plotted; *P* values were calculated using the two-tailed Student's *t* test (***P* < 0.01; **P* < 0.05; NS, not significant). The left panel shows the levels of individual cochaperones in the whole cell and the right panel shows the levels of the same in the nuclear fraction.

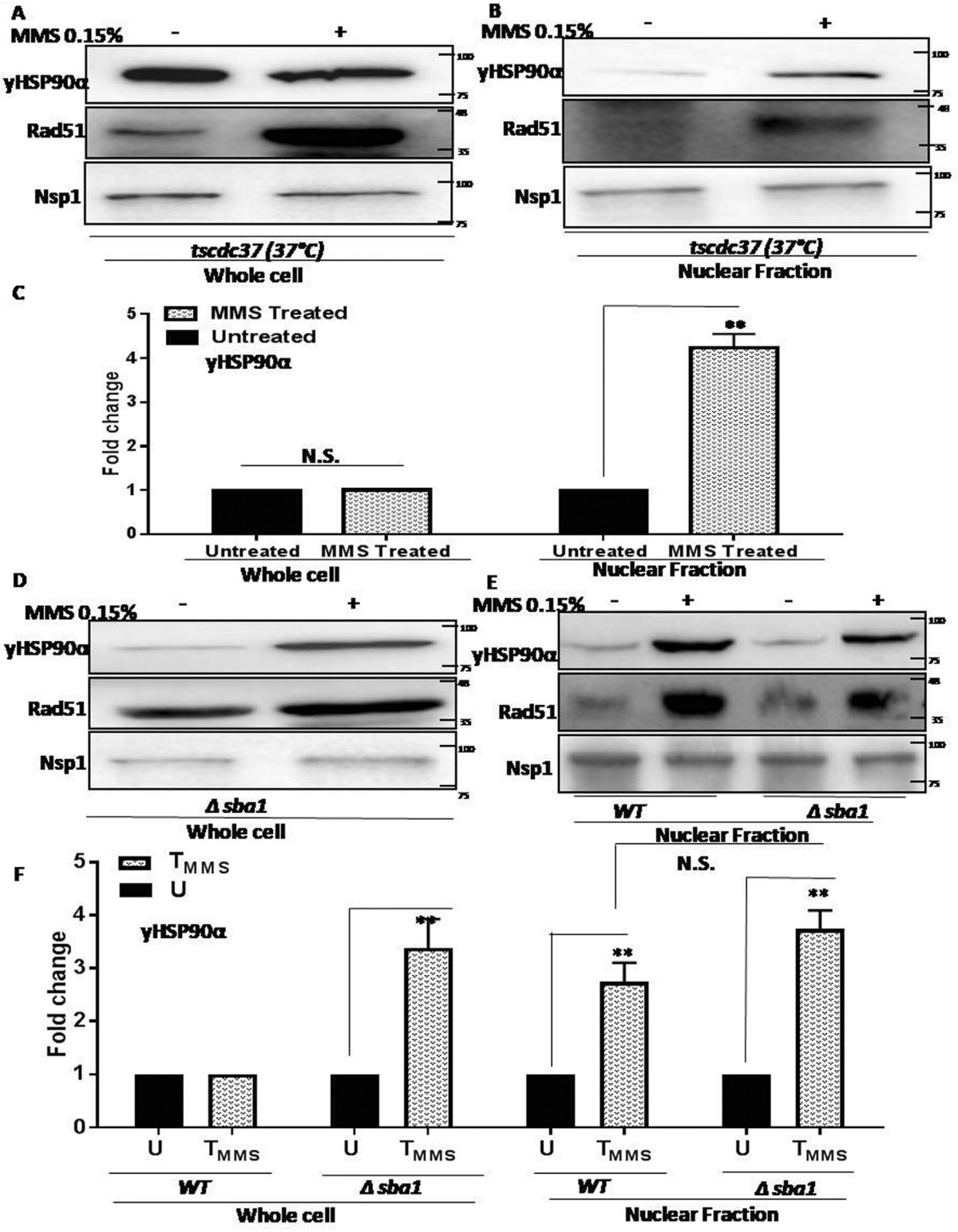

FIGURE 6: yHsp90α transport to the nucleus upon DNA damage is independent of Cdc37 and Sba1. (A) Western blot showing no change in the endogenous level of yHSP90α upon MMS treatment in the temperature-sensitive *tscdc37S14A* strain at nonpermissive temperature (37°C). (B) Western blot shows that *cdc37* loss of function mutation does not alter increased nuclear accumulation of yHSP90α upon MMS treatment. (C) The above experiments (A and B) were repeated with three independent batches of cells and the densitometric image analysis of yHSP90α was presented, *P* values were calculated using the two-tailed Student's *t* test (***P* < 0.01; NS, not significant). (D) In the Δ*sba1* strain endogenous levels of yHSP90α are induced in response to MMS treatment (E) Nuclear fractionation of untreated and MMS-treated wild type and Δ*sba1* strain shows accumulation of yHSP90α in both the wild-type *W303a* and isogenic Δ*sba1* strains. (F) The experiments (D and E) were repeated three times and the mean values (±SD) were plotted, *P* values were calculated using the two-tailed Student's *t* test (***P* < 0.01; N.S., not significant).

expressed in a similar level (Supplemental Figure S2C). Owing to a large molecular weight, the small difference between the molecular weights of GFP-yHSP90α and GFP-yHSP90α$^{(\Delta 211\text{-}259)}$ was not detectable in the Western blot (Supplemental Figure S2C). We studied the recruitment of wild-type (GFP-yHSP90α) and mutant GFP-yHSP90α$^{\Delta(211\text{-}259)}$ on the broken DNA at the second hour post-DNA damage induction, as there was maximum damage at the second hour time point (data not shown). We found no detectable recruitment of GFP-yHSP90α$^{\Delta(211\text{-}259)}$; whereas wild-type GFP-yHSP90α was detected at the *HO* cleavage site, 2-h post-HO induction and IgG precipitation acted as a negative control (Figure 10F). Using Western blot analysis, we determined the levels of the wild type and the mutant protein in the immunoprecipitated samples of the 2-h post-*HO* induction and didn't observe any noticeable difference (Figure 10F, lower panel). We repeated the chromatin immunoprecipitation assay thrice with these two strains and quantified the occupancy of the wild type and the CL-deleted protein at the *HO* cleavage site. We found that the mutant protein was severely defective in its recruitment compared with the WT protein (Figure 10G). To determine the specificity of the CL domain for the nuclear import we have investigated the effect of an ATPase dead mutant, *hsp82T101I* (Nathan and Lindquist, 1995), that also affects the amino-terminal association of yHSP90α (Prodromou *et al.*, 2000). We exposed the mutant strain and the isogenic wild-type strain to MMS and observed that the nuclear import of the mutant protein showed a similar trend as that of the wild-type yHSP90α (Figure 10H). We have estimated the levels of yHSP90α and Rad51 from the *P82a* and mutant strain and presented them graphically (Figure 10I). We observed that both yHSP90α and yHSP90α^{T101I} showed a nearly twofold increased level in the nucleus. However, as expected and reported earlier (Suhane *et al.*, 2014), the level of Rad51 was highly reduced in the mutant strain, although it showed similar fold upregulation in the nucleus upon MMS treatment. Thus using two separation-of-function mutants of yHSP90α our study reveals that the CL domain of yHSP90, which is responsible for the Aha1-mediated conformational rearrangement but not the N-terminal ATPase domain, is required for the nuclear import of yHSP90α.

Loss of nuclear translocation of yHSP90α is correlated with increased sensitivity to MMS

An earlier study in our laboratory demonstrated that the mutant yHSP90α$^{\Delta(211\text{-}259)}$ displays extreme MMS sensitivity and a drastic reduction in Rad51-mediated gene targeting efficiency in yeast (Suhane *et al.*, 2014). Our present study shows that this mutant is defective in DNA damage-induced nuclear import. To study whether DNA damage-induced nuclear import of yHSP90α is directly linked to the protection against MMS-induced cell death, we measured the MMS sensitivity of the mutant yHSP90α$^{\Delta(211\text{-}242)}$ and compared it with the isogenic wild-type and yHSP90α$^{\Delta(211\text{-}259)}$ strains. We observed that the yHSP90α$^{\Delta(211\text{-}242)}$ strain showed similar viability as that of the wild-type strain in the presence of 0.03% MMS (Figure 11), whereas the larger CL-deleted mutant yHSP90α$^{\Delta(211\text{-}259)}$ showed a significant reduction in cell survivability. Hence our study establishes that DNA damage-induced enhanced nuclear accumulation of yHSP90α is a major determinant for providing protective activity against genotoxic stress.

The absence of Aha1 sensitizes the cells to DNA-damaging agents

To further ascertain the importance of Aha1 in DNA repair, we determined the sensitivity of the Δ*aha1* strain toward various DNA-damaging agents. The *WT* and the Δ*aha1* strains were exposed to 0.03% MMS. We found that the absence of Aha1 led to the reduction of cell survivability to 30%, whereas the wild-type strain showed 80% viability (Figure 12A). However, the sensitivity was reversed with the episomal expression of *AHA1* (Figure 12B). We next exposed the *WT* and the Δ*aha1* strains to two different doses of zeocin, namely, 5 and 15 μg/ml. Zeocin, belonging to the bleomycin family of the glycopeptide antibiotic, induces DSB in the chromosome. Our study showed that the absence of Aha1 made the strain more susceptible to zeocin in a dose-dependent manner compared with the isogenic wild-type strain (Figure 12C). However, the sensitivity of zeocin could be reversed by the overexpression of *AHA1* in the Δ*aha1* strain (Figure 12D). Together, this study suggests a direct link between the Aha1 and the genomic stability in the budding yeast.

DISCUSSION

This study has demonstrated for the first time that yHSP90α displays a noncanonical nuclear function during DNA repair in yeast. We observe that cytoplasmic yHSP90α is redistributed to the nucleus in response to DNA damage and this phenomenon is essential for maintaining genome stability. We analyzed two well-characterized CL deletion mutants of yHSP90α that are different by the presence of 17 amino-acid stretches in the linker region (Hainzl *et al.*, 2009). The mutant yHSP90α$^{\Delta(211\text{-}242)}$ shows wild type-like survivability upon MMS treatment and displays an increase in cytoplasm to nuclear accumulation under similar treatment. However, the mutant yHSP90α$^{\Delta(211\text{-}259)}$ fails to get accumulated in the nucleus and displays a fourfold reduction in cell survivability compared with the mutant yHSP90α$^{\Delta(211\text{-}242)}$. This suggests an essential nuclear function of yHSP90α during DNA damage. Comparing the kinetics of the DSB repair and extent of its recruitment, we conclude that yHSP90α may not be involved in the maintenance of the assembly of protein complexes that are recruited immediately after generation of DSB. In our assay, yHSP90α didn't show its immediate association at the first hour, even when the majority of the DNA was broken. Rather, its binding during the second and third hours indicates its probable function during DNA repair. Furthermore, at those time points, yHSP90α shows a significant association up to 4 kb distal position from the cleavage site in a manner similar to that of Rad51. In HR-mediated DSB repair, a long resection occurs at the broken ends that produces a 3′ single-stranded tail region in which the Rad51 protein is coated (Singh *et al.*, 2008). We could detect yHSP90α and Rad51 to the furthest region from the broken side even at a time when 50% breaks still remain unrepaired. As it was previously shown that yHSP90α is physically associated with Rad51 (Suhane *et al.*, 2014), we propose that yHSP90α might play a role in the initiation and maintenance of the Rad51 nucleoprotein filament formation. To establish that further, we studied the extent of chromatin association of the mutant GFP-yHSP90α$^{\Delta(211\text{-}259)}$. We find that this mutant is completely defective in its recruitment to the DSB ends. It is noteworthy that this mutant displays a significant reduction in the MMS-induced Rad51 foci formation and shows a severe defect in Rad51-mediated gene targeting efficiency (Suhane *et al.*, 2014). Hence we conclude that the nuclear import of yHSP90α, followed by its recruitment to the broken ends of DNA, is a prerequisite for effective DNA repair via HR-mediated DNA repair pathway failure of which it can significantly reduce Rad51 nucleoprotein filament formation. It is noteworthy that yHSP90α does not have any DNA binding domain, so it probably associates with chromatin via some unidentified proteins.

It is noteworthy that we didn't determine the kinetics of yHSP90α recruitment at the donor DNA (3′ end of the *URA3*) locus, which is 3 kb away toward the right side of the cleavage junction. The resultant

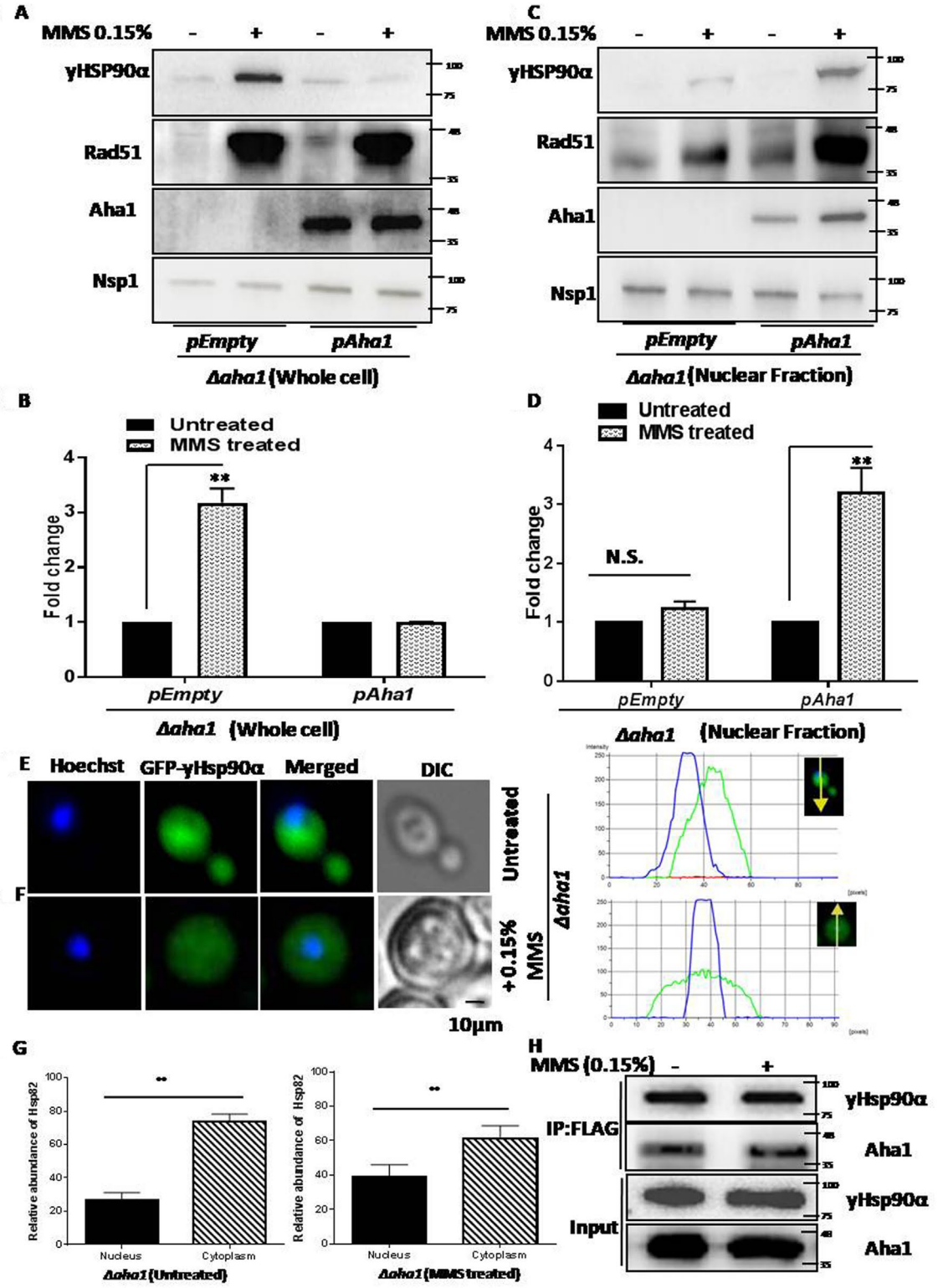

FIGURE 7: yHSP90α transport to the nucleus upon DNA damage is dependent on Aha1. (A) The endogenous level of yHSP90α is induced in Δ*aha1* cells upon 0.15% MMS treatment. There is no difference in its expression between untreated and treated condition upon ectopic expression of *AHA1*. (B) The experiment was repeated multiple times and yHSP90α level was estimated from independent experiments and plotted, *P* values were calculated using the two-tailed Student's *t* test (***P* < 0.01; N.S., not significant). (C) Negligible accumulation of yHSP90α occurs in the nucleus of Δ*aha1* cells upon 0.15% MMS treatment, whereas a marked increase was observed upon ectopic expression of *AHA1* in Δ*aha1* cells under similar conditions. (D) The experiment was repeated multiple times, the nuclear level of yHSP90α was estimated from independent experiments and presented, and *P* values were calculated using the two-tailed Student's *t* test (***P* < 0.01; N.S., not significant). (E) Fluorescence images showing the distribution of GFP-yHsp90α (green) in the whole cell of Δ*aha1* untreated cells. (F) Fluorescence images showing the distribution of GFP-yHsp90α (green) in the

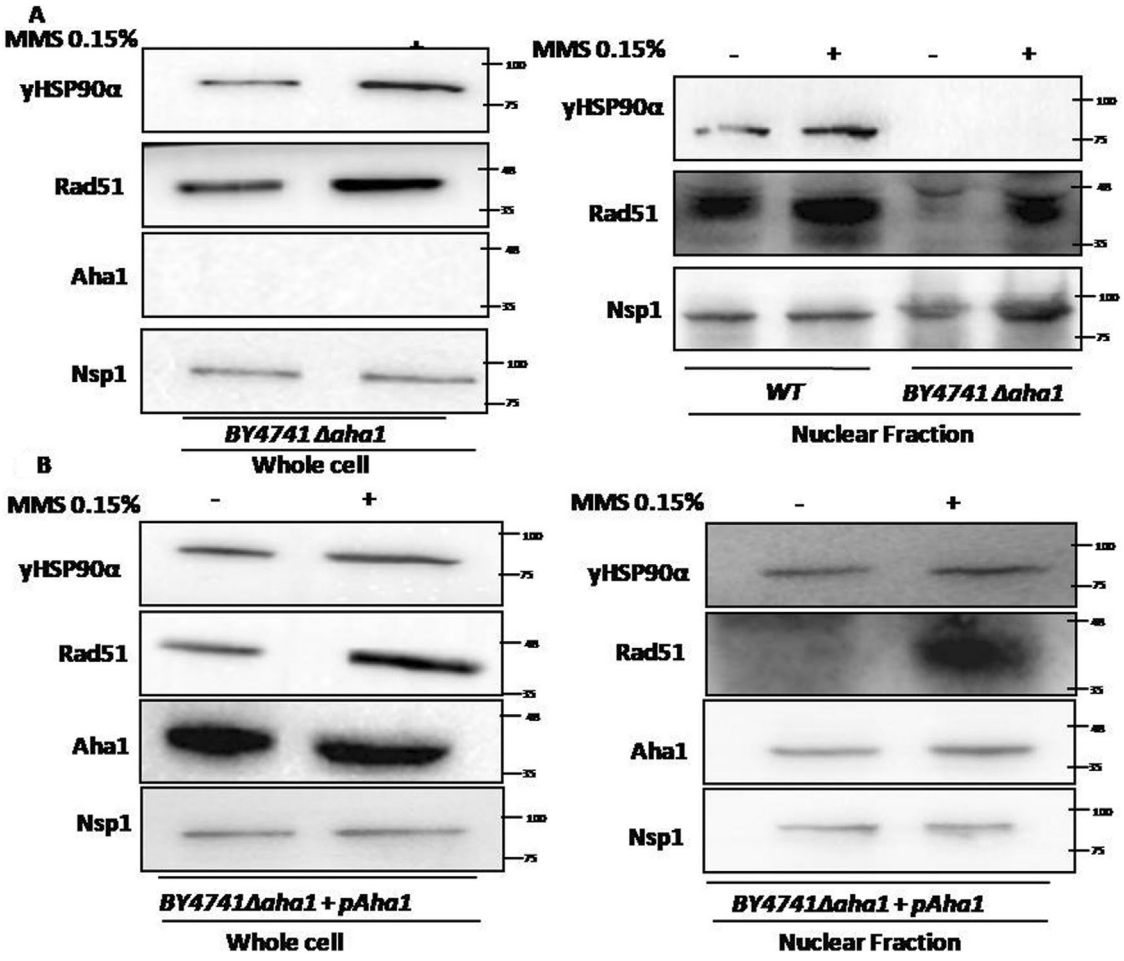

FIGURE 8: yHSP90α transport to the nucleus upon DNA damage is dependent on Aha1 in *BY4741* strain. (A) Western blot analysis shows significant induction of endogenous levels of yHSP90α upon 0.15% MMS treatment in *BY4741Δaha1* strain (left panel). The increased nuclear accumulation of yHSP90α was observed in the WT strain but no signal of yHSP90α was traced in the *BY4741Δaha1* strain upon 0.15% MMS treatment (right panel). (B) The left panel represents the expression of respective proteins in the whole-cell extract of *BY4741Δaha1* strain harboring *AHA1* expression plasmid. The right panel displays that ectopic expression of *AHA1* rescued the defect in nuclear accumulation of yHSP90α in the *BY4741Δaha1* strain. In all the experiments Rad51 served as a control for DNA damage and Nsp1 acted as a loading control.

amplicon during ChIP analysis may be ambiguous as the donor sequence is also identical to that present in the 3′ end of the mutant *ura3*. Hence it will be difficult to delineate the recruitment of yHSP90α between the proximal and distal ends of *HO* cleavage site.

In this study we have identified the structural determinant of yHSP90α that enables its nuclear translocation. yHSP90α adopts multiple conformational changes in its chaperone cycle, one of them being mediated by the ATPase stimulator Aha1 that regulates yHSP90α's allosteric timing. However, how these conformational changes alter its physiological function remains obscure. An earlier biochemical study showed that the conformational flexibility within the amino-terminal and MD of yHSP90α is essential for Aha1-mediated acceleration of ATP hydrolysis of yHSP90α (Hainzl *et al.*, 2009). We speculate that the initial step of Aha1-mediated partially closed conformational rearrangement of yHSP90α could be essential for its nuclear import (Wolmarans *et al.*, 2016). First, the absence of Aha1 completely abrogates the nuclear import of yHSP90α in two different strain backgrounds which are completely reversed on ectopic expression of Aha1. Second, the conformationally rigid CL deletion mutant yHSP90α$^{\Delta(211\text{-}259)}$, which has a 2.5-fold reduction in Aha1-dependent ATPase activity, is fully defective in its nuclear accumulation, although the smaller CL deletion mutant that has wild type-like Aha1-dependent ATPase activity is fully competent in nuclear import. Last, the yHSP90α^{T101I} mutant, which is ATPase-dead mutant

whole cell of Δ*aha1* cells treated with 0.15% MMS. The nucleus (blue) was stained with Hoechst dye. Intensity profiles were derived for all fluorescence experiments using NIS elements AR software. Isogenic WT control are presented in Figure 1, C and D. (G) Relative fluorescence intensities of GFP-yHSP90α in the nucleus and cytoplasm were quantified and the mean values (±SD) were plotted using GraphPad Prism. *P* values were calculated using the two-tailed Student's *t* test (*$P < 0.05$; **$P < 0.01$; N.S., not significant). (H) Western blot showing coimmunoprecipitation of Aha1-FLAG with Hsp90 in the wild-type strain from the untreated and cells treated with 0.15% MMS. Pull down was done using anti FLAG antibody.

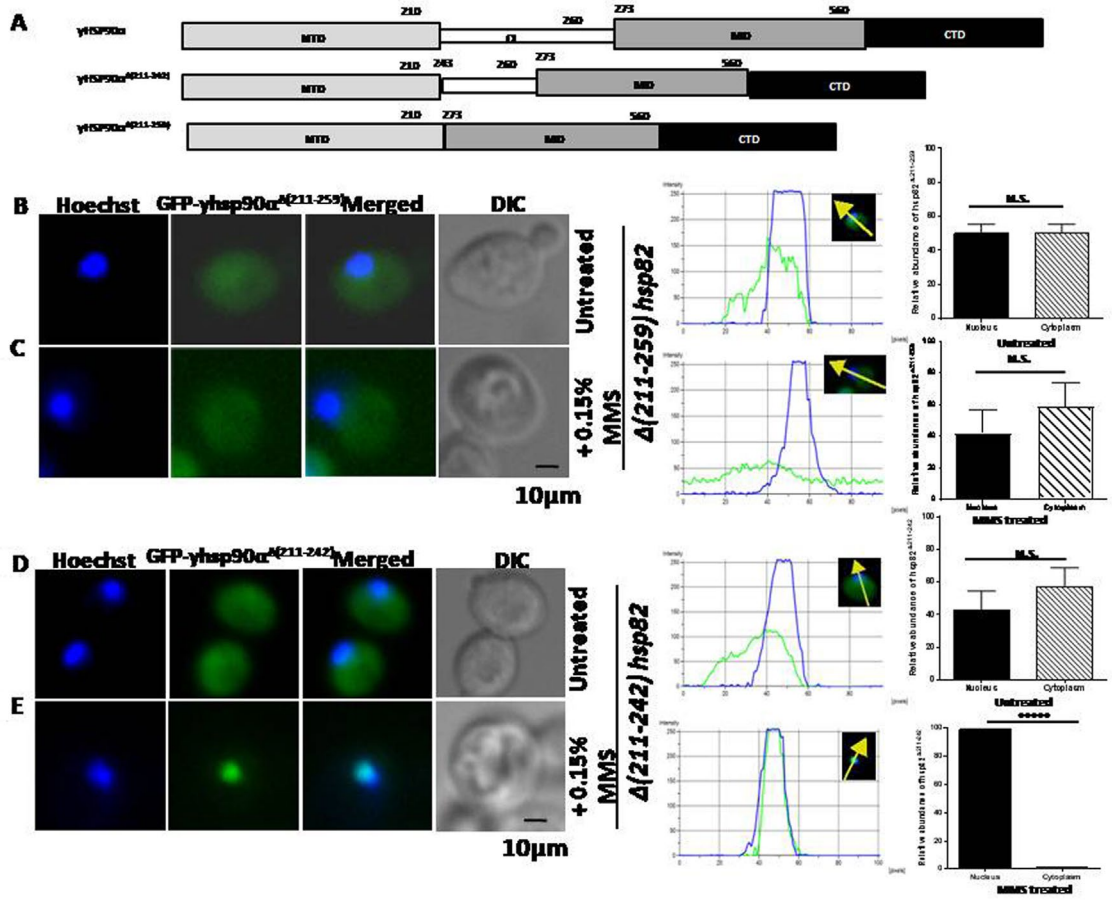

FIGURE 9: The domain responsible for the conformational flexibility between the amino terminal and the MD of yHSP90α is essential for its nuclear translocation upon DNA damage. (A) Schematic representation of wild-type and two CL deletion mutants of yHSP90α. (B) Fluorescence images showing the distribution of GFP-yHsp90α$^{\Delta(211\text{-}259)}$ (green) in the whole cell both in the untreated and (C) in the 0.15% MMS-treated condition. (D) Fluorescence images showing the distribution of GFP-yHsp90α$^{\Delta(211\text{-}242)}$ (green) in the whole cell in the untreated condition but (E) nuclear localization in the 0.15% MMS-treated condition. Intensity profiles were derived for all fluorescence experiments using NIS elements AR software; relative fluorescence intensities of GFP-yhsp90α mutants in the nucleus and cytoplasm were quantified and the mean values (±SD) were plotted using GraphPad Prism. *P* values were calculated using the two-tailed Student's *t* test (*****$P < 0.00001$; N.S., not significant).

with reduced amino-terminal association, shows no defect in nuclear translocation.

While our earlier study (Suhane *et al.*, 2014) demonstrated that the cytoplasmic function of yHSP90α is essential for DNA repair, our present study illustrates that the nuclear function of yHSP90α is also an important determinant for effective DNA repair. It is noteworthy that although the nuclear import of yHSP90α does not depend on its canonical ATPase activity, as seen in the case of *T101Ihsp82*, being an ATPase dead mutant, Rad51 stability is greatly reduced in this mutant background. In our earlier study we reported that this mutant shows severe sensitivity to DNA-damaging agents (Suhane *et al.*, 2014). Thus using two separation-of-function mutants, namely, the *T101Ihsp82* and CL deletion mutant, we demonstrate that the N-terminal domain and the CL domain have distinct functions in DNA repair: while the N-terminal domain is required for the functional stability of the client proteins belonging to the HR pathway, the CL domain is required for the nuclear import of yHsp90, which is a prerequisite for its nuclear role at the time of DSB repair.

It was earlier reported by two independent studies that DNA-PK (Quanz *et al.*, 2012) and ATM (Elaimy *et al.*, 2016) are responsible for the Thr-5/7 phosphorylation of human HSP90α in response to DNA damage. Both enzymes are members of the phosphatidylinositol 3-kinase-like protein kinase (PIKK) family that are the sensors of DNA damage. However, an ortholog of DNA-PK is absent in yeast. Besides, the first 14 amino acids are also absent from yHSP90α. It was never addressed whether there is an increase in the nuclear level of HsHSP90α in response to DNA damage or whether T7/5 phosphorylation is essential for its nuclear import as well as chromatin recruitment. Using human HSP90α and its mutant (T7-A) we have shown that in yeast the nuclear translocation of HsHSP90α is independent of T7 phosphorylation. Further, the ChIP analysis confirms that the association of yHSP90α to the damaged chromatin is independent of the presence of the first 14 amino-acid residues (including T-7). This kind of stress-induced nuclear translocation of yHSP90α was also reported earlier in budding yeast under the condition of glucose starvation (Tapia and Morano, 2010).

We have established for the first time that Aha1 is an important regulator for DNA repair pathway. We observed that *AHA1* was transcriptionally up-regulated in response to DNA damage and showed about a threefold up-regulation in protein level. Using two different strain backgrounds of Δ*aha1*, we showed that Aha1 regulates the nuclear import of yHSP90α. The absence of nuclear

accumulation of yHSP90α in Δ*aha1* strain was fully restored with ectopic expression of *AHA1*. Last, Aha1 deletion shows sensitivity toward genotoxic agents. Although enhanced accumulation of Aha1 was observed into the nucleus under MMS treatment as well as upon induction of single DSB in the genome, its nuclear function during DNA repair has not been addressed in this study. It did not escape our notice that our findings indicate an Aha1-mediated protein homeostasis of yHSP90α under a DNA-damaging condition. The underlying molecular mechanism or its implications need to be explored in future.

In this study we observed that yHSP90α and two of its cochaperones, Sba1 and Aha1, behaved differently upon MMS treatment. yHSP90α is not induced but is redistributed to the nucleus upon DNA damage. Although both Aha1 and Sba1 are induced upon DNA damage, in the case of Aha1, a concomitant increase in its nuclear level was observed, whereas no such increase in the nuclear level of Sba1 was found. We currently do not know the significance of this finding. It could be possible that Aha1 has both nuclear and cytoplasmic roles, whereas Sba1 has a cytoplasmic role during DNA repair.

Presently, it is not understood how a genotoxic stress condition triggers an increase in the nuclear import of yHSP90α. Intriguingly, we find that Hsp90 and Aha1 remain physically associated with each other under normal and DNA-damaging conditions. It is yet to be determined whether some post-translational modifications of yHSP90α and/or Aha1 are necessary for this phenomenon.

We speculate that in a mammalian system also such Aha1-assisted nuclear import of Hsp90α might exist, which needs to be explored in the future. Our finding is very significant as it may open new avenues of research to target Aha1 for arresting HR-mediated DSB repair in cancer cells. Besides, it has been reported earlier in Drosophila and mammals that HSP90α occupies the promoter regions of several coding and noncoding genes and regulates the gene expression in response to external stimuli (Khurana and Bhattacharyya, 2015; Sawarkar *et al*., 2012). If the Aha1 dependence for the nuclear import of HSP90α is universally conserved in higher eukaryotes, then inhibition of Aha1 can be used as a tool to decipher the nuclear function of HSP90α.

MATERIALS AND METHODS

Yeast strains

Strains used in this study have been tabulated in Supplemental Table S1. In *W303a* yeast background, *SBA1* and *CDC37* genes were *MYC* tagged by HR using *HIS* cassettes (Longtine *et al*., 1998) flanked by 40 bp homologous sequence of the upstream and downstream regions of the stop codons of the respective genes to create the *MYC* tagged *SBA1* and *CDC37* strains, namely, *NFY14* and *NFY15*, respectively. For creating the *NFY14* strain, the homologous sequence was added in the primers (OSB389 and OSB390) used for amplifying the *HIS* cassette from the *pFA6a-His-Myc* plasmid. This cassette was then transformed into the *W303a* strain and the cells were grown in a histidine drop-out medium. The *MYC* tagging of *SBA1* was confirmed by PCR using the primer pairs OSB391 and OSB390. For creating the *NFY15* strain, the homologous sequence was added in the primers (OSB398 and OSB399) used for amplifying the *HIS* cassette from the *pFA6a-His-Myc* plasmid. This cassette was then transformed into the *W303a* strain and the cells were grown in a histidine drop-out medium. The *MYC* tagging of *CDC37* was confirmed by PCR using the primer pairs OSB400 and OSB399. *P82a* harboring wild-type *HSP82* expressing vector (*TRP)* was transformed with centromeric *pHCA-hsp82Δ(211-242*) plasmid and the transformed strain was grown in histidine drop-out complete medium to generate the *KRAY16* strain, where the *HSP82* was replaced by the mutant by plasmid shuffling. In the *W303a* yeast background, *AHA1* gene was knocked out by HR using a *HIS* cassette (Longtine *et al*., 1998) flanked by a 40 bp homologous sequence of the upstream and downstream regions of the *AHA1* gene to create the strain *NFY24*. The homologous sequence was added in the primers (OSB273 and OSB274) used for amplifying the *HIS* cassette from the *pFA6a-His* plasmid. This cassette was then transformed into the *W303a* strain and the cells were grown in a histidine drop-out medium. The knockout was confirmed by PCR using the primer pairs OSB275 and OSB274. We used another Δ*aha1* strain which was in the *BY4741* background, purchased from Open Biosystems. Plasmids: Sequences of all the primers used in this paper are tabulated in Supplemental Table S2. Full-out *HSP82, AHA1*, and *RAD51* were amplified using the primer pairs OSB21/OSB22, OSB215/OSB216, and OMKB90/OMKB88, respectively, and individually cloned in the 2-μ vector *pTA* between the *BamH1* and the *Sal1* restriction sites to create *pTA-HSP82, pTA-AHA1*, and *pTA-RAD51*, respectively. We purchased the mammalian expression vector *pcDNA3.1+/C-(K)-DYK* from GenScript, USA, which harbors full-out human *HsHSP90α* with C-terminal *FLAG* tag. We amplified *HsHSP90α-FLAG* using the primer pairs OSB531/OSB539 and subcloned in the centromeric *pHCA* vector (Laskar *et al*., 2011) between the *BamHI* and the *SalI* restriction sites. Two mutants of HsHsp90α, namely, *hsp90αT7A* and the CL deletion mutant *hsp90αΔ(224-279)* were generated by splice overlap extension (SOE) and ultimately subcloned in *pHCA* with C-terminal *FLAG* tag. The CL deletion mutant *hsp82Δ(211-259)* was amplified using the genomic DNA isolated from the *HH1a-p2HG/hsp82Δ(211-259)* strain (Louvion *et al*., 1996; Suhane *et al*., 2014) with the primer pairs OSB21/OSB22. It was subsequently subcloned into the *pTA* vector within the *BamHI* and *SalI* restriction sites. Hsp82 deletion mutant *hsp82Δ(211-242*) was generated by SOE and subsequently subcloned in *pHCA* within the *BamHI* and *SalI* restriction sites. To create the *GFP-Hsp82* fusion constructs, *GFP* was first amplified from the plasmid, *p2U/S65T*, using the primer pair OSB517/OSB518 and subcloned within the *BamH1* restriction site, which is present in the N-terminal end of *HSP82*, *hsp82Δ(211-259)*, and *hsp82Δ(211-242)*. The orientation of *GFP* was checked using *PstI* digestion to create *pTA-GFPhsp82*, *pTA-GFPhsp82Δ(211-259)*, *pHCA-GFPHSP82, pHCA-GFPhsp82Δ(211-259)*, and *pHCA-GFPhsp82Δ(211-242)* fusion constructs, where GFP is fused at the N-terminal end of Hsp82 in all the cases. DNA sequencing (Eurofins) was done to confirm the cloning.

Fluorescence imaging

GFP fluorescence imaging was done using the strains *NFY31, NFY32, NFY33*, and *NFY35* as described earlier (Tapia and Morano, 2010). Typically, the cells were grown until 0.5 OD_{600} in selective media. Half batch of cells were treated with 0.15% of MMS and grown for 2 h along with the untreated batch of cells. *NFY31* was additionally treated with 15 μg/ml nocodazole (Cell Signaling Technology) for 2 h. Nocodazole-induced cell cycle arrest at G2/M was confirmed by visualization of a large number of dumbbell-shaped budding cells under the microscope. Subsequently, the cells were harvested and washed with Milli-Q water. The cells were then treated with 70% ethanol for 1 min at 30°C with shaking and were again washed with water. The cells were resuspended in 100 μl of water and the nuclei of the live cells were stained using Hoechst 33342 (Thermo Fisher Scientific) stain at a concentration of 20 μg/ml for 10 min. The cells were mounted on glass slides using 25% glycerol and were visualized under the 100× objective using a Nikon Eclipse (Ni-E AR) upright fluorescence microscope. The images were

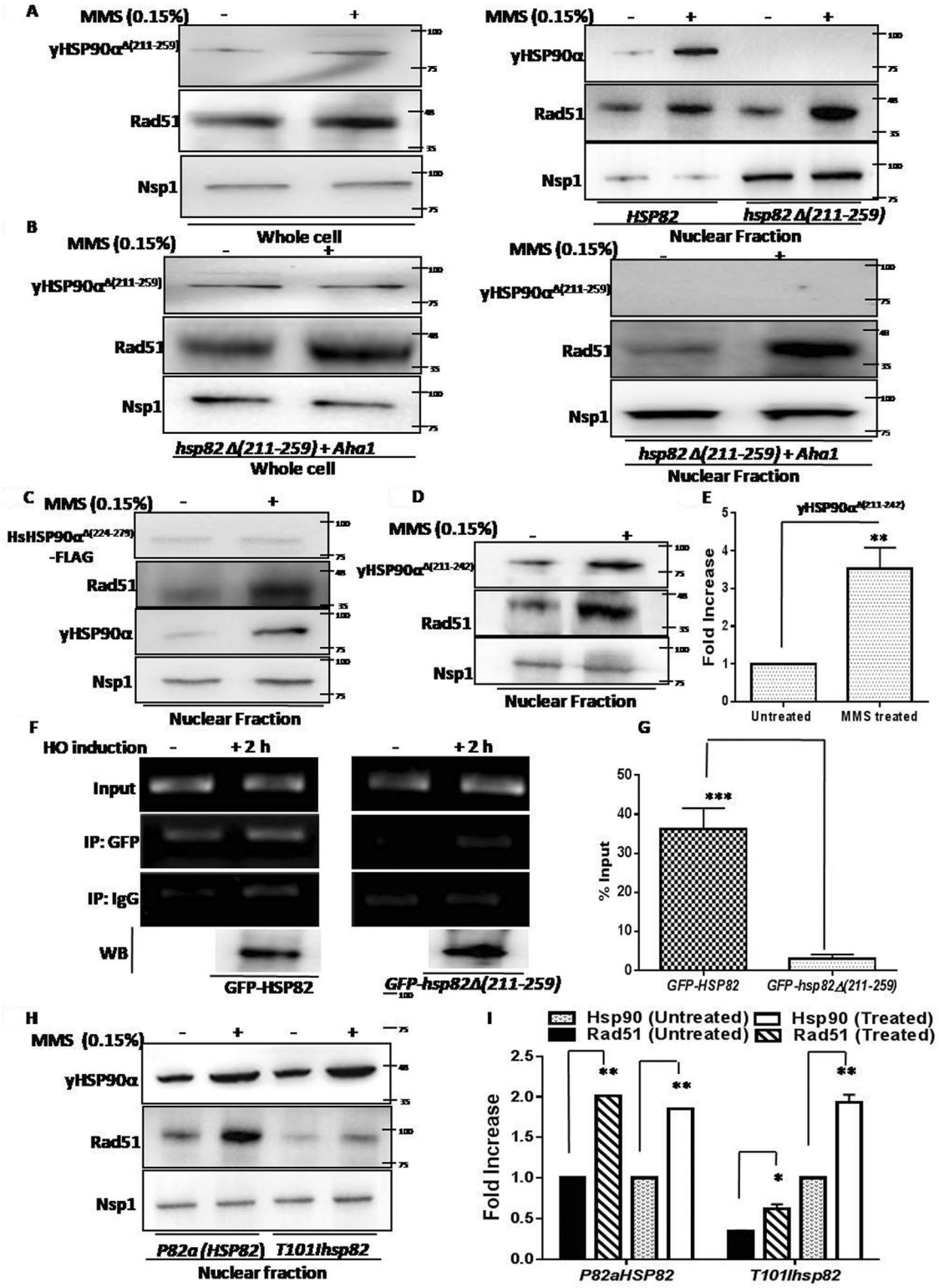

FIGURE 10: The subcellular fractionation of various mutants of yHSP90α in response to DNA damage. (A) Western blots showing the endogenous levels of yHSP90α$^{\Delta(211\text{-}259)}$ in whole-cell extract in the presence and absence of MMS treatment (left panel). Increased nuclear accumulation of yHSP90α^{WT} but no nuclear accumulation of yHSP90α$^{\Delta(211\text{-}259)}$ upon 0.15% MMS treatment was observed (Right panel). (B) Endogenous levels of yHSP90α$^{\Delta(211\text{-}259)}$ in whole-cell extract (left panel) and in nucleus (right panel) shows that no nuclear accumulation of yHSP90α$^{\Delta(211\text{-}259)}$ upon 0.15% MMS treatment even if *AHA1* was overexpressed in the cells. (C) Western blot showing no nuclear accumulation of *FLAG* tagged HsHSP90α$^{\Delta(224\text{-}279)}$ upon 0.15% MMS treatment. (D) Western blot showing increased nuclear accumulation of yHSP90α$^{\Delta(211\text{-}242)}$ upon 0.15% MMS treatment. (E) The experiment was repeated and the quantification of the Western blots showed a fourfold increase in the nuclear level of the mutant yHSP90α$^{\Delta(211\text{-}242)}$ upon MMS treatment. Error bars indicate SD; *P* values were calculated using the two-tailed Student's *t* test (**$P < 0.01$). (F) Chromatin

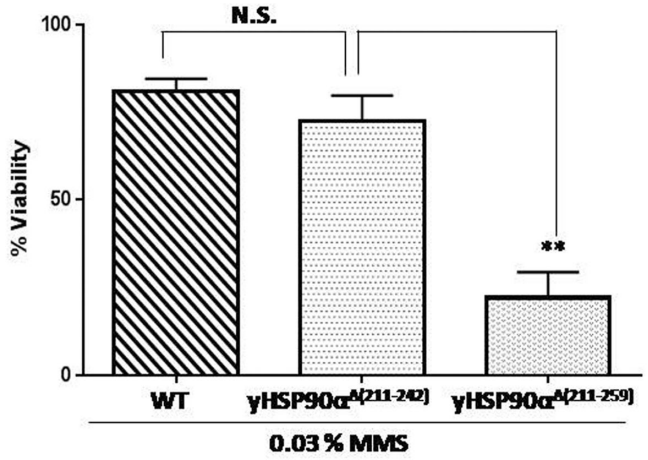

FIGURE 11: Loss of nuclear translocation of yHSP90α is correlated with increased sensitivity to MMS. Percent survivability of yHSP90α$^{\Delta(211\text{-}259)}$, yHSP90α$^{\Delta(211\text{-}242)}$ and isogenic wild-type strains were determined after exposure to 0.03% MMS for 2 h. Error bars indicate ±SD ($n = 3$); *P* values were calculated using the two-tailed Student's *t* test (NS: not significant; $^{**}P < 0.01$).

captured using a monochrome camera (Andor), which were subsequently processed and deconvoluted using NIS elements Advanced Research software (Towa Optics Private Limited). We have performed three independent sets of experiments and analyzed more than 100 cells per condition. The results represent mean ± SD. *P* values were calculated using the two-tailed Student's *t* test.

Indirect immunofluorescence assay

The W303a strain was grown in YPD media until 0.5 OD_{600} and a half batch of cells was treated with 0.15% MMS and both batches were grown for an additional 2 h. The cells were washed and fixed using 4% formaldehyde for 2 h; 10^7–10^8 cells were taken and washed with 1× phosphate-buffered saline (PBS, containing 1 mM dithiothreitol [DTT] and 0.5 mM PMSF). The cells were resuspended in spheroplast buffer (18.2% sorbitol, 1% glucose, 0.2% yeast nitrogen base, 0.2% casamino acids, 25 mM HEPES, pH 7.4, 50 mM Tris, 1 mM DTT) containing YPDS (YPD, 1 M sorbitol) and lyticase. The cells were then incubated for 1.5 h at 30°C with gentle shaking for spheroplasts to form. The slides were meanwhile prepared by coating each well with 0.1% poly-L-lysine and incubated for more than 20 min at room temperature. Extra liquid was removed by aspiration and the wells were dried completely. The fixed yeast spheroplasts were then loaded into each well and allowed to settle for 20 min. Extra liquid was aspirated and the wells were washed with 1× PBS for 5 min. Permeabilization of the cell membrane of the fixed yeast cells was done with a 1:3 mixture of acetone and methanol for 15 min. After washing with 1× PBS, the wells were blocked using 3% bovine serum albumin (BSA) for 1.5 h. The liquid was aspirated and a 1:50 dilution of rabbit anti-Aha1 primary antibody (Invitrogen) diluted in 3% BSA was added to each well and incubated at 37°C for 1 h. After incubation, the extra liquid was aspirated and the wells were washed subsequently with 1× PBS, 1× PBST, and 1× PBS for 15 min each at 37°C. To each well, a 1:250 dilution of the secondary antibody, Goat anti-Rabbit IgG (H+L) Cross-Adsorbed Secondary Antibody, Alexa Fluor 488 (Life Technologies) was diluted in 3% BSA along with 10 µg/ml Hoechst 33342 vital stain (Thermo Fisher Scientific), and the slides were incubated at 37°C for 45 min. All the liquid was then aspirated and the slides were allowed to dry completely after which the samples were mounted using gold antifade (Thermo Fisher Scientific), and the slides were visualized under a 100× objective using a Nikon Eclipse (Ni-E AR) upright fluorescence microscope. The images were captured using monochrome camera (Andor), which were subsequently processed and deconvoluted using the NIS elements Advanced Research software (Towa Optics Private Limited). We have performed three independent sets of experiments and analyzed more than 100 cells per condition. The results represents mean ± SD. *P* values were calculated using the two-tailed Student's *t* test.

Site-directed mutagenesis

The CL deletion mutants, *hsp82Δ(211-242)* and human *hsp90αΔ(224-279)-FLAG*, were created using splice overlap extension PCR. To generate the *hsp82Δ(211-242)* deletion mutant, yeast genomic DNA was used as a template, and the full-length gene was amplified in two fragments to delete the desired region. For amplifying the first and second fragments, primer sets OSB21/OSB537 and OSB538/OSB22 were used, respectively. Finally, *hsp82Δ(211-242)* deletion was generated by annealing the first two PCR products followed by a third PCR using the primer set OSB21/OSB22. To generate the human *hsp90αΔ(224-279)* deletion mutant, the full-length gene was amplified as two fragments, one using the primer set OSB531/OSB533 and the other using the OSB534/OSB539 primer pair. The two PCR products were denatured, allowed to hybridize with each other, and subsequently amplified using the primer pair OSB531/OSB539 to create the human *hsp90αΔ(224-279)* deletion. To create the human *T7Ahsp90α* mutant by site-directed mutagenesis, the *pcDNA3.1+/C-(K)-DYK* vector was used as a template along with the primer set OSB535/OSB539. The codon *ACC* was changed to *GCT* within the primer OSB535 to create the human *T7Ahsp90α* mutant. All the mutants were confirmed by sequencing.

immunoprecipitation (ChIP) assay were done using NA14 strain harboring either *GFP* tagged y*HSP90α* vector or *GFP* tagged CL-deleted mutant y*hsp90α* vector. Anti GFP antibody was used to pull down WT and CL-deleted mutant y*HSP90α* from uninduced and 2 h *HO* induced samples. The pellet fraction was PCR amplified; the recruitment of *GFP* tagged yHSP90α^{WT} was detected at 2 h of HO induction while the recruitment of the mutant protein was not detected. The samples were normalized with respect to input. The lower panel shows the Western blotting of the IP sample, which detects the presence of comparable amount of the wild-type and the mutant protein in the +2 h galactose treated samples. (G) The ChIP assay was repeated twice ($n = 2$) and the occupancy of the GFP-Hsp82^{WT} and the GFP-Hsp82$^{\Delta(211\text{-}259)}$ at the *HO* cleavage site were plotted. Error bars indicate SD; *P* values were calculated using the two-tailed Student's *t* test ($^{***}P < 0.001$) (H) Western blot showing increased nuclear accumulation of yHSP90α in *P82a* strain as well as in an isogenic *hsp82T101I* strain upon 0.15% MMS treatment. Rad51 levels were very less in the *hsp82T101I* strain as expected, nonetheless it shows significant up-regulation upon MMS treatment. (I) Quantification of the Western blots from multiple experiments shows significant increase in the nuclear level of both yHSP90α and Rad51 in the WT and the mutant strain. Error bars indicate SD; *P* values were calculated using the two-tailed Student's *t* test ($^{**}P < 0.01$; $^{*}P < 0.05$).

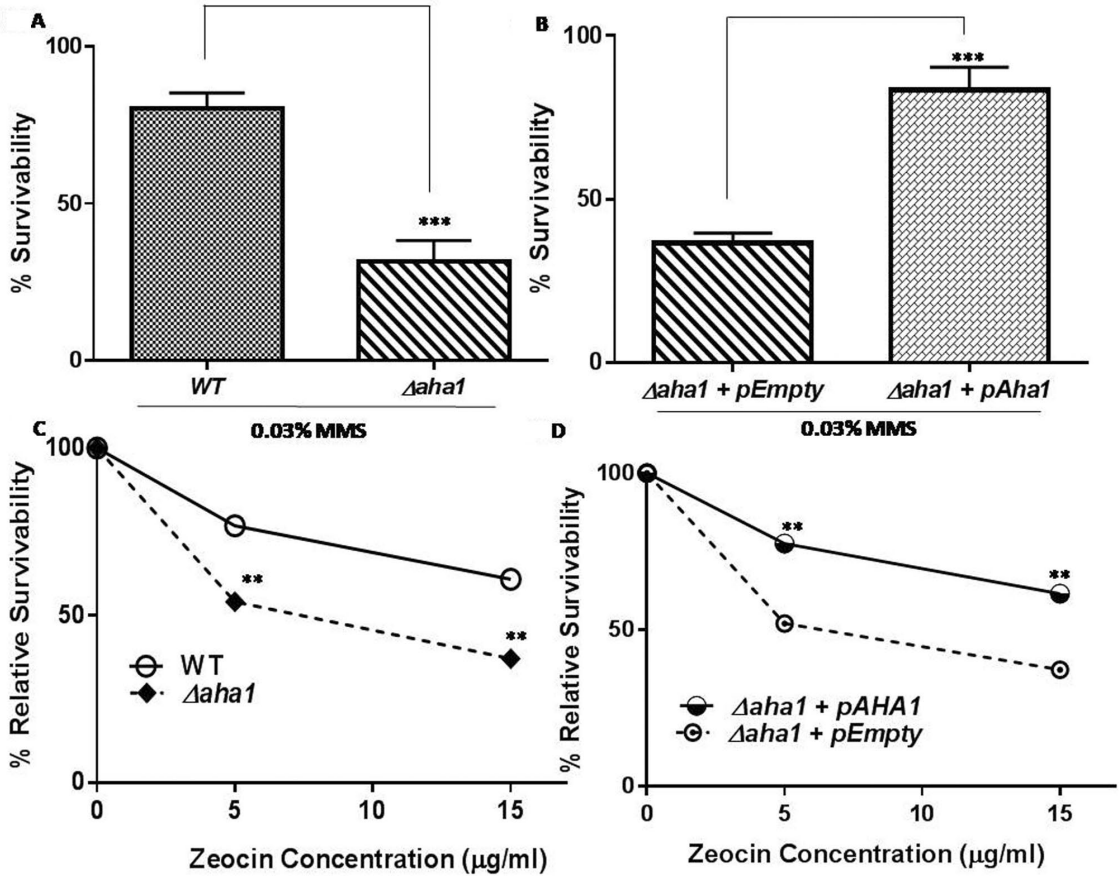

FIGURE 12: Aha1 deletion sensitizes the cells to DNA-damaging agents. (A) Return to growth experiments were conducted with the wild-type and isogenic Δ*aha1* strain. Percentage survivability upon 0.03% MMS treatment were plotted relative to that of untreated cells. (B) Return to growth experiments were conducted with the Δ*aha1* cells harboring *AHA1* expressing vector or empty *pTA* vector upon exposure to 0.03% MMS. Each treatment was repeated three times, and the mean value (±SD) was plotted; *P* values were calculated using the two-tailed Student's *t* test (*****P* < 0.0001; ****P* < 0.001). (C) *WT* and Δ*aha1* strains were exposed to two doses of zeocin (5 μg/ml and 15 μg/ml) and their relative survivability was plotted. Δ*aha1* strain showed greater susceptibility toward zeocin compared with the *WT* strain. The experiment was repeated three times and the mean values were plotted; *P* values were calculated using the two-tailed Student's *t* test (***P* < 0.01). (D) Zeocin sensitivity of Δ*aha1* strain harboring empty plasmid was reversed in *AHA1* expressing Δ*aha1* strain. The mean values were plotted (*n* = 3); *P* values were calculated using the two-tailed Student's *t* test (***P* < 0.01).

Cellular fractionation

The nuclear fractionation was done with wild-type, *NA14* (Agmon *et al.*, 2009), Δ*sba1* (*SLY6*), Δ*aha1* (*NFY24*), and *tscdc37S14A* strains (grown at restrictive temperature 37°C). Similar fractionations were also performed with the strains carrying wild-type *HsHsp90α-FLAG* (*KRAY15*) and those carrying the human *hsp90αT7A-FLAG* (*KRAY17*) and human *hsp90αΔ(224-279)-FLAG* (*KRAY18*). To measure whether the nuclear level of yHSP90α depends on Aha1, we did nuclear fractionation of Δ*aha1* strain carrying empty plasmid (*NFY26*) and that carrying *AHA1* overexpression plasmid (*NFY27*). Finally, various mutants of *hsp82*, namely, *HH1a-p2HG/hsp82Δ(211-259), T101Ihsp82,* and *hsp82Δ(211-242)* (*KRAY16*), and the isogenic control strain *P82a* were also subjected to nuclear fractionation. Typically, cells were grown until 0.5 OD_{600} in selective media. A half batch of cells were treated with 0.15% of MMS and continuously grown at 30°C for 2 h along with the untreated batch of cells. In the *NA14* strain, DNA damage was induced as a specific double-strand DNA break at an *HO* restriction site by inducing *HO* endonuclease within the cell using 3% galactose (Agmon *et al.*, 2009). After DNA damage, 100 OD_{600} cells were harvested and washed with PBS containing DTT and PMSF. In each case, cells were then incubated with spheroplast buffer (18.2% sorbitol, 1% glucose, 0.2% yeast nitrogen base, 0.2% casamino acids, 25 mM HEPES, pH 7.4, 50 mM Tris, 1 mM DTT) for 15 min at 30°C with gentle shaking. After incubation, cells were resuspended in spheroplast buffer containing YPDS (YPD, 1 M sorbitol) and lyticase enzyme. It was then allowed to grow at 30°C with gentle shaking for 1.5 h. Again, YPDS was added into spheroplast and spun at 4000 rpm for 10 min. Washing of the spheroplast was performed with ice-cold YPDS followed by spinning at 4000 rpm for 5 min. Spheroplast was resuspended in ice-cold sorbitol and spun at 4000 rpm for 5 min. Ultimately the spheroplast was resuspended in 5 ml of buffer N (25 mM K_2SO_4, 30 mM HEPES, pH 7.6, 5 mM $MgSO_4$, 1 mM EDTA, 10% glycerol, 0.5% NP40, 3 mM DTT, 1% protease inhibitor cocktail) and homogenized by giving 20 strokes under chilled conditions. The homogenized spheroplast was spun at 2000 rpm at 4°C for 15–20 min to pellet down the cell debris. We pelleted down the nuclei at 6000 rpm for 25 min at 4°C. This nuclear fraction sample was then resuspended in 50 μl of buffer N. The sample was then boiled for 10 min and used for the Western blotting analysis.

Coimmunoprecipitation

The *KRAY29* strain was grown in the selective media without tryptophan until 0.5 at OD_{600}. A half batch of cells was treated with 0.15% of MMS and grown at 30°C for 2 h along with the untreated batch of cells. Cells were harvested and the pull down was done by using anti-FLAG antibody as described previously (Suhane *et al.*, 2019). After coimmunoprecipitation, the relative association of Hsp90 with Aha1 was analyzed by Western blotting.

Western blotting

Western blot was done to study protein levels in whole-cell protein samples or nuclear fractions. Protein samples were loaded onto a SDS polyacrylamide gel. Polyvinylidene difluoride membrane was used for the Western blot as described earlier (Laskar *et al.*, 2011). The primary antibodies used were mouse anti-Act1 antibody (Abcam), rabbit anti-Rad51 (Abcam), mouse anti-Hsp82 antibody (Calbiochem), rabbit anti-Aha1 antibody (Invitrogen), mouse Anti-DDDDK tag antibody (Abcam), and rabbit anti-GFP antibody (Abcam) at 1:5000 dilutions. For subcellular fractionation, we used mouse anti-Nsp1 antibody (Abcam) as loading control at 1:5000 dilution. For secondary antibodies, horseradish peroxide–conjugated anti-rabbit antibody (Promega) and anti-mouse antibody (Promega) were used at 1:10,000 dilution. The Western blots were developed using chemiluminescent detection system (Thermo Fisher Scientific). Every experiment was repeated at least three times and band intensities were quantified by using ImageJ software. Mean relative densities were plotted using GraphPad Prism.

Repair kinetics of a single double-strand DNA break

NA14 cells (Agmon *et al.,* 2009) were grown in YPD media in the presence of 3% glycerol until 0.3 at OD_{600}; 60 OD of cell were harvested (untreated or 0 h) and the remaining cells were treated with 3% galactose for different time points (1, 2, 3, and 4 h). At each time point, 5 OD_{600} of cells were harvested. The yeast cells were disrupted using 0.3 g glass beads and 200 µl breaking buffer (2% Triton X-100, 1% SDS, 10 mM NaCl, 10 mM Tris [pH 8], 1 mM EDTA [pH 8]). The genomic DNA was subsequently extracted from the yeast cells using PCIA. The extracted genomic DNA was treated with RNase and resuspended in 30 µl 1× Tris-EDTA solution. The kinetics of a single double-stranded break repair at the *HO* restriction site were monitored by PCR using the primers OSB289 and KanB1 which are specific to the upstream and downstream regions of the *HO* restriction site.

Chromatin immunoprecipitation

The strains, *NFY21, NFY22, NFY23, NFY25 and KRAY19*, were grown in the selective media without tryptophan until 0.3 at OD_{600} in the presence of 3% glycerol; 60 OD of cell were taken out and treated with 1% formaldehyde for 15 min (untreated or 0 h) and the remaining cells were treated with 3% galactose for different time points (1, 2, 3, and 4 h). At each time point, 60 OD_{600} of cells were taken out and treated with 1% formaldehyde for 15 min each. Formaldehyde-mediated protein cross-linking was stopped using 2.5 M glycine. After formaldehyde treatment, each set of cells was harvested and washed with 1× PBS. ChIP assay was performed for each set of cells as described earlier (Laskar *et al.*, 2014). Pull down was done with each set using 10 µg anti-Hsp90 antibody (Calbiochem), 10 µg anti-Rad51 antibody (Abcam), 10 µg anti-Aha1 antibody (Abcam), and 10 µg anti-GFP antibody (Abcam) to precipitate HSP90α, Rad51, Aha1, and GFP bound DNA fragments, respectively, at each time point. Recruitment of HSP90α, Rad51, and Aha1 was then monitored at the *HO* cleavage proximal site and up to –5 kb distal position by PCR using the immune precipitate and input DNA samples for each time point. Recruitment near the broken region was studied by subjecting the samples to PCR using the primers OSB519 and OSB520 while recruitment to the 1, 2, 3, 4, and 5 kb away from the *HO* cleavage side toward the left direction was measured using the primers OSB567/OSB568, OSB569/OSB570, OSB571/OSB572, OSB573/OSB574, and OSB575/OSB576, respectively. Samples were subjected to electrophoresis on 2% agarose. For a negative control, ChIP was performed with IgG antibody. We amplified 300 bp at the 3′ end of *ACT1* using OSB14 and OSB16 (Laskar *et al.*, 2011), which was used as a normalization control.

MMS sensitivity assay

W303a, NFY24, NFY26, and *NFY27* strains were tested for MMS-induced DNA damage sensitivity. All strains were grown in YPD medium overnight at 30°C. The next day, secondary culture was grown until 0.5 OD_{600} at 30°C. After OD_{600} reached to 0.5, the culture was divided into two sets. One set of cells was treated with 0.03% (vol/vol) of methyl-methane-sulfonate (MMS) (Sigma Aldrich) and grown at 30°C for 2 h and another set was continuously grown at 30°C for 2 h without MMS. After that, the cells were washed twice and serially diluted, and 1000 cells of each culture were spread on respective selective media or YPD plates. The plates were incubated at 30°C for 40 h and the colonies obtained were counted in both treated and untreated conditions. Subsequently, the percentage survivability was calculated using the following formula: % survivability = [(number of cells grown on MMS plate)/(number of cells grown on untreated plate)] *100.

Zeocin sensitivity assay

W303a, *NFY24, NFY26*, and *NFY27* strains were tested for zeocin-induced DNA damage sensitivity. All strains were grown in YPD medium for overnight at 30°C. The next day, secondary culture was grown until 0.5 OD_{600} at 30°C. After OD_{600} reached 0.5, the culture was divided into two sets. One set of cells was treated with 5 µg/ml or 15 µg/ml zeocin (Invitrogen) and grown at 30°C for 1 h, and another set was continuously grown at 30°C for 1 h without zeocin. After that the cells were washed twice and serially diluted and 1000 cells of each culture were spread on respective selective media or YPD plates. The plates were incubated at 30°C for 40 h, the colonies obtained were counted, and the percentage survivability was calculated.

Real-time RT-PCR

The W303α strain was grown at 30°C until the OD_{600} reached to 0.5. It was subsequently exposed to 0.15% MMS for 2 h. Total RNA was isolated from the untreated and MMS-treated cells using the acid phenol method as described previously (Suhane *et al.*, 2014). Further cDNA was synthesized using reverse transcriptase (Omni Script; Qiagen, Hilden, Germany) as described previously (Suhane *et al.*, 2014). The primer pair, OSB 14 and OSB 16, was used to amplify 307 bp at the 3′ end of *ACT1* transcript. To amplify 326 bp at the 3′ end of *RAD51*, the primer pair OSB 44 and OSB 45 was used. Similarly, to amplify 291 bp at the 3′ end of the *AHA1* transcript, the primer pair OSB 216 and OSB 394 was used. Finally, to amplify 276 bp at the 3′ end of *SBA1*, the primer pair OSB 391 and OSB 445 was used. For real-time RT-PCR, cDNA was diluted (1:50) and used for PCR using a Takara TB Green RT-PCR kit as described earlier (Suhane *et al.*, 2014). The mean values (±SD) from three independent experiments were plotted using GraphPad Prism 6 software.

ACKNOWLEDGMENTS

The authors thank Mrinal K Bhattacharyya, University of Hyderabad, for critical reading of the manuscript. N.F. was supported by the Senior Research Fellowships from Council for Scientific and Industrial Research (CSIR), India. K.R. and P.S. were supported by the Senior Research Fellowships from Council for Scientific and Industrial Research (CSIR), India. The plasmid *p2U/S65T.Hsp82* was a kind gift from Didier Picard, University of Geneva. The Δ*aha1* strain (BY4741 background) and the temperature-sensitive strains *cdc37S14A* were a kind gift from Atin K. Mandal, Bose Institute, Kolkata.

REFERENCES

Agmon N, Pur S, Liefshitz B, Kupiec M (2009). Analysis of repair mechanism choice during homologous recombination. Nucleic Acids Res 37, 5081–5092.

Ali MMU, Roe SM, Vaughan CK, Meyer P, Panaretou B, Piper PW, Prodromou C, Pearl LH (2006). Crystal structure of an Hsp90-nucleotide-p23/Sba1 closed chaperone complex. Nature 440, 1013–1017.

Andriuskevicius T, Kotenko O, Makovets S (2018). Putting together and taking apart: assembly and disassembly of the Rad51 nucleoprotein filament in DNA repair and genome stability. Cell Stress 2, 96–112.

Aylon Y, Kupiec M (2004). DNA repair: the yeast paradigm. DNA repair 3, 797–815.

Caplan AJ, Ma'ayan A, Willis IM (2007). Multiple kinases and system robustness: a link between Cdc37 and genome integrity. Cell Cycle 6, 3145–3147.

Echtenkamp FJ, Zelin E, Oxelmark E, Woo JI, Andrews BJ, Garabedian M, Freeman BC (2011). Global Functional Map of the p23 Molecular Chaperone Reveals an Extensive Cellular Network. Mol Cell 43, 229–241.

Elaimy AL, Ahsan A, Marsh K, Pratt WB, Ray D, Lawrence TS, Nyati MK (2016). ATM is the primary kinase responsible for phosphorylation of Hsp90α after ionizing radiation. Oncotarget 7, 82450–82457.

Hainzl O, Lapina MC, Buchner J, Richter K (2009). The Charged Linker Region is an important regulator of Hsp90 function. J Biol Chem 284, 22559–22567.

Khurana N, Bhattacharyya S (2015). Hsp90, the concertmaster: tuning transcription. Front Oncol 5, doi:10.3389/fonc.2015.00100.

Kimura Y, Rutherford SL, Miyata Y, Yahara I, Freeman BC, Yue L, Morimoto RI, Lindquist S (1997). Cdc37 is a molecular chaperone with specific functions in signal transduction. Genes Dev 11, 1775–1785.

Laskar S, Bhattacharyya MK, Shankar R, Bhattacharyya S (2011). HSP90 controls SIR2 mediated gene silencing. PLoS One 6, e23406.

Laskar S, Sheeba K, Bhattacharyya MK, Nair AS, Dhar P, Bhattacharyya S (2014). Heat stress induced Cup9 dependent transcriptional regulation of Sir2. Mol Cell Biol 35, doi: 10.1128/MCB.01046-14.

Li J, Soroka J, Buchner J (2012). The Hsp90 chaperone machinery: Conformational dynamics and regulation by co-chaperones. Biochim Biophys Acta 1823, 624–635.

Li X, Heyer WD (2008). Homologous recombination in DNA repair and DNA damage tolerance. Cell Res 18, 99–113.

Longtine MS, Mckenzie A, Demarini DJ, Shah NG, Wach A, Brachat A, Philippsen P, Pringle JR (1998). Additional modules for versatile and economical PCR-based gene deletion and modification in Saccharomyces cerevisiae. Yeast 14, 953–96.

Louvion JF, Warth R, Picard D (1996). Two eukaryote-specific regions of Hsp82 are dispensable for its viability and signal transduction functions in yeast. Proc Natl Acad Sci 93, 13937–13942.

Lundin C, North M, Erixon K, Walters K, Jenssen D, Goldman ASH, Helleday T (2005). Methyl methanesulfonate (MMS) produces heat-labile DNA damage but no detectable in vivo DNA double-strand breaks. Nucleic Acids Res 33, 3799–3811.

Mader SL, Lopez A, Lawatscheck J, Luo Q, Rutz DA, Hernandez APG, Sattler M, Buchner J, Kaila VRI (2020). Conformational dynamics modulate the catalytic activity of the molecular chaperone Hsp90. Nat Commun 11, https://doi.org/10.1038/s41467-020-15050-0.

Nathan DF, Lindquist S (1995). Mutational analysis of Hsp90 function: interactions with a steroid receptor and a protein kinase. Mol Cell Biol 15, 3917–3925.

Prodromou C, Panaretou B, Chohan S, Siligardi G, O'Brien R, Ladbury JE, Roe SM, Piper PW, Pearl LH (2000). The ATPase cycle of Hsp90 drives a molecular 'clamp' via transient dimerization of the N-terminal domains. EMBO J 19, 4383–4392.

Quanz M, Herbette A, Sayarath M, Koning LD, Dubois T, Sun JS, Dutreix M (2012). Heat shock protein 90α (Hsp90α) is phosphorylated in response to DNA damage and accumulates in repair foci. J Biol Chem 287, 8803–8815.

Sawarkar R, Sievers C, Paro R (2012). Hsp90 globally targets paused RNA polymerase to regulate gene expression in response to environmental stimuli. Cell 149, 807–818.

Siligardi G, Panaretou B, Meyer P, Singh S, Woolfson DN, Piper PW, Pearl LH, Prodromou C (2002). Regulation of Hsp90 ATPase activity by the co-chaperone Cdc37p/p50cdc37. J Biol Chem 277, 20151–20159.

Singh TR, Ali AM, Busygina V, Raynard S, Fan Q, Du CH, Andreassen PR, Sung P, Meetei AR (2008) BLAP18/RMI2, a novel OB-fold-containing protein, is an essential component of the Bloom helicase–double Holliday junction dissolvasome. Genes Dev 22, 2856–2868.

Suhane T, Bindumadhavan V, Fangaria N, Nair AS, Tabassum W, Muley P, Bhattacharyya MK, Bhattacharyya S (2019). Glu-108 in ScRad51 is critical for DNA damage induced nuclear function. mSphere 4, doi: 10.1128/mSphere.00082-19.

Suhane T, Laskar S, Advani S, Roy N, Varunan S, Bhattacharyya D, Bhattacharyya S, Bhattacharyya MK (2014). Both charged linker region and ATPase domain of Hsp90 are essential for Rad51 dependent DNA repair. Eukaryot Cell 14, 64–77.

Sun L, Prince T, Manjarrez JR, Scroggins BT, Matts RL (2012). Characterization of the interaction of Aha1 with components of the Hsp90 chaperone machine and client proteins. Biochimica et Biophysica Acta 1823, 1092–1101.

Tapia H, Morano KA (2010). Hsp90 nuclear accumulation in quiescence is linked to chaperone function and spore development in yeast. Mol Biol Cell 21, 63–72.

Tsutsumi S, Mollapour M, Prodromou C, Lee CT, Panaretou B, Yoshida S, Mayer MP, Neckers LM (2012). Charged linker sequence modulates eukaryotic heat shock protein 90 (Hsp90) chaperone activity. Proc Natl Acad Sci USA 109, 2937–2942.

Wolmarans A, Lee B, Spyracopoulos L, LaPointe P (2016). The Mechanism of Hsp90 ATPase Stimulation by Aha1. Sci Rep 6, doi:10.1038/srep33179.